Published online 18 July 2016

Nucleic Acids Research, 2016, Vol. 44, No. 20 ***9681–9697***
doi: 10.1093/nar/gkw652

H2B ubiquitination regulates meiotic recombination by promoting chromatin relaxation

Zhiliang Xu[1,2], Zhenhua Song[1,2], Guoping Li[3], Huayu Tu[1,2], Weixiao Liu[1], Yujiao Liu[4], Pan Wang[1], Yuanting Wang[1,2], Xiuhong Cui[1], Chao Liu[1,2], Yongliang Shang[1,2], Dirk G. de Rooij[5], Fei Gao[1] and Wei Li[1,*]

[1]State Key Laboratory of Stem Cell and Reproductive Biology, Institute of Zoology, Chinese Academy of Sciences, Beijing 100101, China, [2]University of the Chinese Academy of Sciences, Beijing 100049, China, [3]The Key Laboratory of Geriatrics, Beijing Hospital and Beijing Institute of Geriatrics, Ministry of Health, Beijing 100730, China, [4]College of Marine Life, Ocean University of China, Qingdao 266003, China and [5]Reproductive Biology Group, Division of Developmental Biology, Department of Biology, Faculty of Science, Utrecht University, Padualaan 8, 3584 Utrecht, the Netherlands

Received January 23, 2016; Accepted July 11, 2016

ABSTRACT

Meiotic recombination is essential for fertility in most sexually reproducing species, but the molecular mechanisms underlying this process remain poorly understood in mammals. Here, we show that RNF20-mediated H2B ubiquitination is required for meiotic recombination. A germ cell-specific knockout of the H2B ubiquitination E3 ligase RNF20 results in complete male infertility. The *Stra8-Rnf20*$^{-/-}$ spermatocytes arrest at the pachytene stage because of impaired programmed double-strand break (DSB) repair. Further investigations reveal that the depletion of RNF20 in the germ cells affects chromatin relaxation, thus preventing programmed DSB repair factors from being recruited to proper positions on the chromatin. The gametogenetic defects of the H2B ubiquitination deficient cells could be partially rescued by forced chromatin relaxation. Taken together, our results demonstrate that RNF20/Bre1p-mediated H2B ubiquitination regulates meiotic recombination by promoting chromatin relaxation, and suggest an old drug may provide a new way to treat some oligo- or azoospermia patients with chromatin relaxation disorders.

INTRODUCTION

Meiotic recombination enables the reciprocal exchange of genetic materials between parental homologous chromosomes and ensures faithful chromosome segregation during meiosis in sexually reproductive organisms. Disorders in meiotic recombination often lead to meiotic arrest or chromosome segregation failure, and finally results in dire consequences such as infertility (1,2). Meiotic recombination is initiated by the formation of programmed DNA double-strand breaks (DSBs) (Supplementary Figure S1), which are mainly repaired by homologous recombination. Programmed DSBs are induced by the evolutionarily conserved SPO11 protein at the leptotene stage (3). The programmed DSB repair pathway is initiated by the activation of several conserved kinases, including ATM and ATR, in a process that is similar to DSB repair in somatic cells (4). Upon activation, ATM and ATR phosphorylate histone H2AX at serine 139 (termed γH2AX) (5) and BRCA1 (6). Autophosphorylated ATM (termed pATM) then phosphorylates NBS1 at the DSB sites (7). NBS1 is a component of the MRN complex, which contains MRE11 and RAD50; MRE11 has 3′-to-5′ exonuclease activity and endonuclease activity and cooperates with NBS1/Xrs2 and RAD50 to generate the single strands at the DSB sites (8). The single strands are protected by the RPA complex (RPA1, 2 and 3) from degradation, and they will invade other homologous chromosome strands with the help of RAD51 and DMC1 which replace RPA at the zygotene stage (9). After single strand invasion, the programmed DSB is repaired by meiotic homologous recombination via homologous chromosome synapsis and crossover/noncrossover. Meiotic homologous chromosome synapsis depends on the formation of the synaptonemal complex (SC complex), which contains SYCP1, SYCP2 and SYCP3 (10). SYCP3 and SYCP2 are lateral elements of the SC complex and are distributed along the chromosome axis. SYCP1 is the central element that links two homologous chromosomes for pairing and the formation of the chiasmata at the pachytene stage (10). After pairing and synapsis, the crossovers between the homologous chromosomes are finished by MLH1 and other

*To whom correspondence should be addressed. Tel: +86 10 64807529; Fax: +86 10 64807316; Email: leways@ioz.ac.cn

molecules (11), and then the spermatocytes enter into the diplotene stage and diakinesis stages, finally exiting the long meiotic prophase. Although an overall molecular model has been built, the detailed mechanisms underlying meiotic recombination remain elusive.

It has been proposed that meiotic recombination is evolved from mitotic homologous recombinational repair (HRR) (12). This hypothesis largely depends on the fact that these two pathways share some components. Recently, protein ubiquitination has emerged as a critical factor in double-strand DNA break repair and genome stability (13). Among the ubiquitination-related factors, RAD6 (14), UBR2 (15), CUL4A (16) and HEI10 (17) are involved in meiotic recombination, whereas UBC13 (18), RNF8 (19) and RNF168 (20) are not required for this process. Recently, it was reported that histone H2B ubiquitination (H2Bub) is involved in HRR in mammalian somatic cells (21,22). In mammalian cells, with the help of WAC (WW domain containing adaptor with coiled-coil), H2Bub is mediated by E2 RAD6 and the E3 ligase RNF20/RNF40 heterodimer (23). RNF20 and RNF40 are RING finger proteins, and their RING domains are critical for the formation of a heterodimeric complex and the stability of each other (24). RNF20/RNF40 exists as a tetramer containing two copies of each protein (25). They are reported to be required for the transcription of some genes (26–28), and play vital roles in some fundamental biological processes such as stem cell differentiation (29–31) and tumorigenesis (26,32). Whether H2Bub or its related E3 ligase involved in meiotic recombination or spermatogenesis in mammals is unknown.

Here, we show that RNF20 is required for meiotic recombination by promoting chromatin relaxation at the zygotene and pachytene stages. We generated an *Rnf20*$^{Flox/Flox}$ mouse and created a meiosis-specific *Rnf20*-knockout mouse by mating *Rnf20*$^{Flox/Flox}$ mice with *Stra8-Cre* mice. Once *Rnf20* was knocked out in the germ cells, the spermatocytes were arrested at the pachytene stage due to impaired programmed DSB repair. Further investigation revealed that the depletion of RNF20 in germ cells affected chromatin relaxation by reducing H2B ubiquitination, thus preventing the recruitment of programmed DSB repair factors to the proper positions on the chromosome. Meiotic recombination and the gametogenetic defect of the H2B ubiquitination deficient cells could be partially rescued by chloroquine treatment. Taken together, we identified RNF20 as a chromatin binding protein during meiosis, demonstrated that RNF20-mediated H2B ubiquitination regulates meiotic recombination by promoting chromatin relaxation, and revealed that an old drug might provide a new treatment for some oligo- or azoospermia patients with chromatin relaxation disorders during meiotic recombination.

MATERIALS AND METHODS

Generation of *Rnf20*-conditional-knockout mice

Conditional knockout (cko)-targeting vectors were constructed using recombineering to introduce *LoxP* sites and selection markers into BAC DNA by a novel recombineering approach adapted from Liu *et al.* (33). Briefly, a 7.7-kb *Rnf20* fragment containing exons 2, 3 and 4 was subcloned from the 129 SVEV BAC library into the PL253 vector by gap repair with homology arms via recombineering. The resulting DNA sequence was confirmed by sequencing. Then, the *LoxP* sites were introduced into this subcloned genomic region via two targeting rounds using the neomycin (*Neo*) cassettes from the PL452 and PL451 vectors. To insert the first single 5′ *LoxP* site, a *LoxP*-flanked neomycin resistance (*Neo*) cassette (PL452) was introduced into the subcloned genomic region via homology, and the *Neo* cassette was subsequently removed by electroporating the targeted plasmid DNA into EL350 cells, which had been previously induced for Cre expression by growth in an arabinose-containing medium for 1 h. Using the same procedure, an *Frt-neo-Frt-LoxP* cassette from PL451, which was homologous to the region 3′ of *Rnf20* intron 4, was inserted to generate the complete cko-targeting vector. To avoid the introduction of undesired mutations during the recombination process, both targeted regions were confirmed by sequencing.

The cKO-targeting vector was then linearized with NotI and electroporated into R1 ES cells using standard procedures. The resultant G418-resistant clones were genotyped by PCR, and the PCR products were sequenced both to verify the junction regions, including the first *LoxP* site, the second *LoxP* site and two *Frt* sites (neo cassette), and to ensure that no other sequence alterations had occurred. Correct ES-targeting clones were then injected into C57BL/6 blastocysts, which were then implanted into pseudo-pregnant CD1 foster females. The resultant male chimeras were identified by coat color and mated to C57BL/6 mice to assess germ line transmission. After germ line transmission of the targeted (*Neo*) allele, the resultant heterozygous *Rnf20*$^{+/Flox\text{-}Neo}$ mice were then mated to transgenic mice expressing the FLP recombinase (34) to induce excision of the *Neo* marker. *Rnf20*$^{Flox/Flox}$ mice were generated by intercrossing *Rnf20*$^{Flox/+}$ heterozygous mice. Homozygous *Rnf20*$^{Flox/Flox}$ mice were crossed with transgenic mice expressing the CRE recombinase under the control of the *Stra8* promoter (35) to generate *Rnf20*$^{Flox/Flox}$*;Stra8-Cre* (referred to as *Stra8-Rnf20*$^{-/-}$) mice. Genotyping PCR for *Rnf20* was performed using the following primers: forward: GCTGTAAGAGTTCTTAATGTATG, and reverse: GG CTTGTCACACAAG CATGAGCATC. The PCR conditions were as follows: 94°C for 5 min; 35 rounds of 94°C for 30 s, 58°C for 30 sec, and 72°C for 1 min; and 72°C for 5 min.

All animal experiments were approved by the Animal Research Panel of the Committee on Research Practice of the University of the Chinese Academy of Sciences.

Antibodies

Rabbit antibody to SYCP3 (ab150292), rabbit antibody to RPA1 (ab87272) and rabbit antibody to VASA (ab13840) were purchased from Abcam (Cambridge, UK). Mouse antibody to γH2AX (05-636), mouse antibody to ATMps1981 (05-740) and mouse antibody to H2Bub (05-1312) for immunohistochemistry were purchased from Merck Millipore (Darmstadt, Germany). For immunoblotting, rabbit antibody to H2Bub (5546s) was purchased from Cell Signaling Technology (Danvers, MA). Mouse antibody to MLH1 (51-1327GR) was purchased from BD Pharmingen (SanDiego, CA). Rabbit antibody to SYCP1

(NB300-228c), rabbit antibody to MRE11 (NB100-142) and rabbit antibody to NBS1 (NB100-143) were purchased from Novus Biologicals (Littleton, CO). Mouse antibody to SYCP3 (SC-74569), goat antibody to ATR (SC-1187), goat antibody to BRCA1 (SC-1553), rabbit antibody to RAD51 (SC-8349), rabbit antibody to DMC1 (SC-22768), mouse antibody to PLZF (SC-28319) were purchased from Santa Cruz Biotechnology (Dallas, TX, USA). Rabbit antibody to RNF20 (21625-1-AP) for immunoblotting was purchased from Proteintech (Chicago, IL, USA). Rabbit antibody to H3K14ac (BE3225) and mouse antibody to H3K9me2 (BE3016) were purchased from Easybio (Beijing, China). Mouse antibody to Mouse Sperm Protein sp56 (55101) was purchased from QED Bioscience Inc. (San Diego, CA). Goat FITC-conjugated secondary antibody to rabbit, donkey FITC-conjugated secondary antibody to mouse, rabbit TRIRC-conjugated secondary antibody to goat, goat TRIRC-conjugated secondary antibody to mouse and horseradish peroxidase (HRP)-conjugated secondary antibodies were purchased from Zhong Shan Jin Qiao (Beijing, China). Alexa Fluor®680-conjugated goat secondary antibody to mouse (A21057) and Alexa Fluor® 680-conjugated rabbit secondary antibody to goat (A21088) for immunoblotting were purchased from Invitrogen (Carlsbad, CA), IRDye® 800CW-conjugated goat secondary antibody to rabbit (926-32211) for immunoblotting were purchased from LI-COR (Lincoln, NE).

The polyclonal antibody to RNF20 for immunofluorescence and the polyclonal antibody to RNF40 were generated as follows: cDNA fragments encoding *hRnf20* and *hRnf40* were inserted into pET28a and pGEX4T1, respectively. His-tagged RNF20 protein or GST-tagged RNF40 protein were extracted from BL21-CodonPlus (DE3) cells, solubilized in phosphate-buffered saline (PBS) and purified by Ni Sepharose High Performance (17-5268-02, GE Healthcare, Pittsburgh, PA, USA) or Glutathione Sepharose High Performance (17-5279-02 GE Healthcare, Pittsburgh, PA, USA) chromatography, respectively. The recombinant proteins were dialyzed in PBS and used to immunize rabbits. Polyclonal antibodies to RNF20 and RNF40 were affinity purified on antigen-coupled SulfoLink Coupling Gel (20402, Thermo Fisher, Waltham, MA).

Breeding assays

Breeding assays with *Rnf20*$^{Flox/Flox}$ and *Stra8-Rnf20*$^{-/-}$ male mice were carried out as described previously (36). Briefly, each examined male mouse (8 weeks) was caged with two wild-type (CDI strain) female mice (6–8 weeks), and their vaginal plugs were checked every morning. The number of pups produced by each pregnant female was counted within a week after birth. Each male was tested through at least six cycles of this breeding assay.

TUNEL assays

TUNEL assays were carried out using the In Situ Cell Death Detection Kit (Roche Diagnostics, 11684795910, Rotkreuz, Switzerland) as described in our previous paper (36).

Tissue collection and histological analysis

Testes and caudal epididymides were dissected immediately following euthanasia. The tissues were then fixed in Bouin's fixative overnight at 4°C, dehydrated in an ethanol series, and embedded in paraffin wax. Then, 5-μm sections were cut with a microtome. Following deparaffinization and rehydration, the sections were stained with hematoxylin and Periodic acid Schiff (PAS) or eosin for histological analysis. Images were collected with a Nikon inverted microscope with a charge coupled device (CCD) (Nikon, Eclipse Ti-S, Tokyo, Japan).

Immunohistochemistry (IHC)

Paraffin sections were fixed with 4% paraformaldehyde and rinsed in PBS three times. Then, the sections were boiled for 15 min in sodium citrate buffer for antigen retrieval. After blocking with 5% bovine serum albumin (BSA), each section was incubated with a primary antibody at 4°C overnight and then washed in PBS three times. The sections were then treated with 3% H_2O_2 to eliminate internal peroxidase activity. After three PBS washes, the sections were stained with an horseradish peroxidase (HRP)-conjugated secondary antibody. Finally, the sections were stained with 3,3′-diaminobenzidine (DAB), and the nuclei were stained with hematoxylin. Images were collected using a Nikon inverted microscope with a CCD (Nikon, Eclipse Ti-S, Tokyo, Japan).

Spermatocyte surface spreading

Spermatocyte surface spreading was performed using the drying-down technique previously described by Peters et al (37). Briefly, the testes were dissected, and the tubules were washed in phosphate-buffered saline (PBS), pH 7.4, at room temperature. Then, tubules were placed in a hypotonic extraction buffer containing 30 mM Tris, 50 mM sucrose, 17 mM trisodium citrate dihydrate, 5 mM EDTA, 0.5 mM DTT and 0.5 mM phenylmethylsulfonyl fluoride (PMSF), pH 8.2, for 30–60 min. Subsequently, the tubules were torn to pieces in 100 mM sucrose, pH 8.2, on a clean glass slide and were pipetted repeatedly to make a suspension. The cell suspensions were placed on slides containing 1% paraformaldehyde (PFA), pH 9.2, and 0.15% Triton X-100. The slides were dried for at least 2 h in a closed box with high humidity. Finally, the slides were washed twice with 0.4% Photoflo (Kodak, 1464510, Rochester, NY) for 2 min and dried at room temperature.

Immunofluorescence

Testes were embedded in an optimum cutting temperature compound (SAKURA Tissue-Tek® O.C.T. Compound, 4583, Torrance, CA) and cut in 6-μm sections using a microtome-cryostat (Leica, CM1950, Wetzlar, Germany). Testis sections were fixed with 4% paraformaldehyde (PFA) for 15 min and washed in PBS three times (pH 7.4). Then, the sections were treated with 0.3% Triton X-100 for 10 min and rinsed in PBS 3 times. After blocking with 5% bovine serum albumin for 30–60 min, the slides were incubated

with a primary antibody in 1% BSA containing 0.1% Triton X-100 at 4°C overnight. After three rinses in PBS, the sections were incubated with a fluorescein isothiocyanate-conjugated secondary antibody at a dilution of 1:200 for 1 h at 37°C. Next, the nuclei were stained with 4′,6-diamidino-2-phenylindole (DAPI). For spread immunofluorescence, the spread preparations were rinsed 2 times for 10 min in ddH_2O and 3 times for 5 min in PBS, blocked in 5% BSA for 1 h, incubated overnight at 4°C with the corresponding primary antibodies, and stained as described above. For paraffin sections, the sections were boiled for 15 min in sodium citrate buffer for antigen retrieval and then processed as described above. Images were collected immediately using a TCS SP8 confocol microscope (Leica, TCS SP8, Wetzlar, Germany).

Isolation of mouse spermatogenic cells

Spermatogenic cells were isolated using a method previously described by Bellve with a slight modification (38). Briefly, testes from adult *Rnf20*$^{Flox/Flox}$ and *Stra8-Rnf20*$^{-/-}$ mice were removed and decapsulated. The seminiferous tubules were tore into small pieces and incubated in 8 ml PBS containing 1 mg/ml collagenase (Sigma, C5138, St. Louis, MO, USA) and 1 mg/ml hyaluronidase (Sigma, H3506, St. Louis, MO) at 37°C for 6 min with gentle shaking. After pipetting, the dispersed seminiferous tubules and cells were incubated at 37°C for 5 min with gentle shaking. Then, the cells were collected by centrifugation at 200 × *g* for 5 min at 4°C, washed once with PBS, resuspended in 15 ml PBS containing 0.25% Trypsin and 1 mg/ml DNase I, and incubated at 37°C for 5 min with gentle shaking. Thereafter, the cells were collected and washed with PBS containing 0.5% BSA. After filtration through a 40 μm Nylon Cell Strainer, the cells were separated by sedimentation velocity at unit gravity at 4°C, using a 2–4% BSA gradient in PBS. The cell fractions were bottom-loaded in a volume of 300 ml. An aliquot of each fraction was examined by light microscope to assess cellular purity and cell type identity. The fractions containing the expected cell type (zygotene and pachytene spermatocytes) and purity (≥ 90%) were pooled together and identified with immunofluorescence against with PLZF, SYCP3 or sp56.

Immunoblotting

Tissue extracts were prepared using a Dounce homogenizer in cold RIPA buffer (25 mM Tris–HCl, pH 7.6, 350 mM NaCl, 1% Nonidet P-40, 1% sodium deoxycholate, and 0.1% sodium dodecyl sulfate) supplemented with 1 mM phenylmethylsulfonyl fluoride and a protein inhibitor cocktail (Roche Diagnostics, 04693116001, Rotkreuz, Switzerland). Spermatocytes isolated from testes were resuspended in cold RIPA buffer as described above. After transient sonication, the cell lysate was incubated on ice for 30 min. The samples were centrifuged at ∼14 000 ×*g* for 15 min to pellet the cell debris, and the supernatant was transferred to a new tube for further analysis. Protein concentration was determined using the Bio-Rad Bradford protein assay. Protein lysates were separated via SDS-PAGE and electrotransferred to a nitrocellulose membrane. After incubation with primary and secondary antibodies, the membrane was scanned using an ODYSSEY Sa Infrared Imaging System (LI-COR Biosciences, Lincoln, NE, USA).

Micrococcal nuclease (MNase) sensitivity assay

The assay was performed as previously described with a minor modification (39). Briefly, isolated spermatocytes were incubated in a hypotonic buffer (10 mM Hepes, pH 7.9, 10 mM KCl, 1.5 mM $MgCl_2$, 0.34 M sucrose, 10% glycerol and 1 mM dithiothreitol (DTT)) supplemented with 0.1% Triton X-100. After washing in hypotonic buffer without Triton X-100, the cell nuclei were digested with 4 U MNase in 200 μl reaction buffer (15 mM Tris–HCl, pH 7.4, 60 mM KCl, 0.25 M sucrose, 1 mM $CaCl_2$, and 0.5 mM DTT) at 25°C for the indicated period of time. The reaction was terminated by adding an equal volume of 2× TNESK buffer (20 mM Tris–HCl, pH 7.4, 0.2 M NaCl, 2 mM EDTA, and 2% SDS) with freshly added proteinase K (0.2 mg/ml). The samples were then incubated 2 h or overnight at 37°C, and genomic DNA was purified and separated by electrophoresis in a 1.2% agarose gel. The intensity of each lane was quantified using the GIS 1D software.

Yeast cell nuclei MNase sensitivity assay was performed as described with a few modifications (40). In brief, yeast cells were harvested at 4 h in the sporulation medium. After incubated in preincubation buffer (0.7 M β-mercaptoethanol, 3 mM EDTA, 20 mM Tris–HCl (pH 8.0)) at 30°C for 15min with shaking, the yeast cells were washed in 1 M srobitol and incubated in the 0.1 mg/ml zymolyase 100T at 30°C for 30 min with shaking. The resultant spheroplasts were collected by centrifugation at 3500 rpm for 5 min. After incubation in the lysis buffer (18% (w/v) Ficoll 400, 10 mM KH_2PO_4, 10 mM K_2HPO_4, 1 mM $MgCl_2$, 0.25 mM EGTA, 0.25 mM EDTA) for 5 min, the solution was centrifuged at 12 000 rpm at 4°C for 30 min. The supernatant was carefully removed and the crude nuclear suspension was digested with MNase in the buffer A (10 mM Tris–HCl (pH 8.0), 150 mM NaCl, 5 mM KCl, 1 mM EDTA) which contained 5 mM $CaCl_2$ at 37°C for the indicated period of time. The reaction was terminated by adding 25 mM EDTA (pH 8.0), 1% (w/v) SDS and 0.06 mg/mL Proteinase K, then each sample was incubated at 55°C for 2 h to overnight. Five M potassium acetate was added and incubated for 15 min. After centrifugation at 12 000 rpm for 10 min to remove cell debris, the supernatant was subjected to phenol–chloroform extraction and isopropanol precipitation for DNA purification. The pellet was dissolved in 50 μl of ddH_2O. After digestion of RNA with the DNase free of RNase with 30 min at 37°C, genomic DNA was separated by electrophoresis in 1.2% agarose gel. The intensity of each lane was consecutively quantified by using the GIS 1D software.

Testicular chloroquine injection

Chloroquine (C6628, Sigma, St. Louis, MO) was injected into mouse testes using a previously described method (41) with minor modifications. Briefly, 6-week-old *Rnf20*$^{Flox/Flox}$ and *Stra8-Rnf20*$^{-/-}$ mice were anaesthetized with avertin (T48402, Sigma, St. Louis, MO) through intraperitoneal injection, and 30 μl of a chloroquine solution in 0.9% NaCl

was then slowly injected into the efferent ductules of the testes with a needle attached to a 50-μl microinjector. After injection of the testes, mice were fostered for another 3 weeks. Testes and epididymides were then dissected and fixed for normal histological analysis and immunofluorescence; spermatozoa from the epididymides were sampled to examine their number.

Yeast strains, sporulation and chloroquine treatment

All yeast strains in this study were SK1 derivatives and were described in Supplementary Table S1. Strain with *bre1* deletion was constructed by standard procedure (42). The *H2BFLAG* and *H2BK123R* yeast strains were constructed as previous reported with some modifications (43,44). Firstly, *HTB2* gene was deleted and *HTB1* gene was cloned into a YEP vector with an HA epitope at the N-terminus of HTB1, then it was transformed into the *HTB2* deletion strain, after which the endogenous *HTB1* was knocked out. Next, the *HTB1* was cloned into a pRS424 vector with FLAG epitope at the C-terminus (pRS424-*H2B-FLAG*). Then pRS424-*H2B-FLAG (TRP1)* was introduced into the YEP-*HA-H2B (URA3)* strains. Finally, the yeast strains that contained the pRS424-*H2B-FLAG (TRP1)* and YEP-*HA-H2B (URA3)* were cultured on 5-fluoroorotic acid plates to evict the YEP-*HA-H2B (URA3)* plasmid. For *H2BK123R* yeast strain, lysine-to-arginine substitution mutations were introduced at conserved ubiquitination site (K123) in the HTB1 gene by PCR based mutagenesis combined with homologous recombination *in vivo*. Strains that contained the recombined plasmid (pRS424-*H2B-K123R -FLAG*) were selected after growth on 5-ß uoroorotic acid plates.

Yeast cells were grown in YPD medium (1% yeast extract, 2% peptone, 2% glucose) or YPA medium (1% yeast extract, 2% peptone, 2% potassium acetate). For sporulation, yeast cells were grown overnight in liquid YPD medium and diluted in liquid YPA medium to an OD_{600} of 0.3 and cultured for 10 h at 30°C. Then cells were harvested and resuspended in sporulation medium (2% potassium acetate) to OD_{600} of 1.9 and sporulated at 30°C for different lengths of time. In the treatment of chloroquine to the *bre1Δ* or *H2BK123R* mutant strains experiments, chloroquine was added into the sporulation medium for the first 4 h and then removed to test its effects on sporulation.

Sporulation was assayed by the microscopic examination of cultures that had been incubated in SPM (sporulation medium) for 24 h. Approximately five hundreds cells per culture were counted and the percentage of cells that had formed asci was scored. The nuclear DNA was stained by DAPI, visualized and counted using a Nikon inverted microscope (Nikon, Eclipse Ti-S, Tokyo, Japan).

Real-time PCR

Real-time PCR was performed with a Roche Light Cycler® 480II System. Total RNA was extracted from isolated spermatocytes with a Trizol Kit. cDNA was synthesized using the PrimeScript RT Reagent Kit (TaKaRa, RR037A, Kusatsu, Janpan). Amplification was performed in a 10-μl reaction with 5 μl 2× EvaGreen mix (Applied Biological Materials Inc., MasterMix-S, Richmond, Canada), 0.8 μl of each primer (10 nmol/l), 2 μl sample cDNA, and 2.2 μl ddH_2O. The real-time PCR was initiated at 95°C for 10 min, followed by 40 cycles of denaturation for 5 sec at 95°C, annealing for 30 s at 60°C, and elongation for 60 s at 72°C. Fluorescence signals were collected at 72°C during the elongation step. Each DNA amplification was performed in triplicate. The results were analyzed using Light Cycle 480SW 1.5.1.

Statistical analysis

All data are presented as the mean ± SEM. The statistical significance of the difference between the mean values for the different genotypes was examined using Student's *t*-test with a paired two-tailed distribution. The data were considered significant when $P < 0.05$ (*), 0.01(**) or 0.001(***).

RESULTS

H2B ubiquitination mainly occurs in spermatocytes

To study the potential role of H2Bub during spermatogenesis, we first used immunohistochemistry to investigate the localization of H2Bub in the seminiferous tubules of mice. We found that H2B ubiquitination mainly occurred in spermatogonia and spermatocytes (Supplementary Figure S2A). Then we isolated the spermatogonia, spermatocytes and round spermatids from the mouse testis to detect the expression of RNF20, which is the major E3 ligase for H2B ubiquitination (Supplementary Figure S2B and C). Consistent with the localization of H2Bub, the expression of RNF20 was high in spermatocytes but low in round spermatids and absent in spermatozoa which were isolated from mouse cauda epididymidis (Supplementary Figure S2D). These results suggest that H2B ubiquitination is dynamically regulated during spermatogenesis and that H2Bub and RNF20 might participate in the regulation of meiosis.

Germ cell-specific knockout of *Rnf20* results in male infertility

To explore the potential function of H2B ubiquitination during spermatogenesis, we generated an $Rnf20^{Flox/Flox}$ mouse via a highly efficient recombineering-based method (33). Briefly, *LoxP* and the neomycin resistance cassette were sequentially inserted into the introns flanking exons 2–4 of the *Rnf20* gene (Supplementary Figure S3A). After electroporation, the targeted embryonic stem (ES) cell clones were screened and verified by multiple rounds of PCR (Supplementary Figure S3B). The positive clones of the targeted ES cells were microinjected into blastocysts and then transplanted into the uteri of mice to produce chimeric offsprings (Supplementary Figure S3C). The neomycin cassette between the *Frt* sites was removed after crossing with FLP mice to generate $Rnf20^{Flox/Flox}$ mice (Supplementary Figure S3A).

To determine whether RNF20 is required for meiosis, $Rnf20^{Flox/Flox}$ mice were mated with *Stra8-Cre* mice (35) to produce $Rnf20^{Flox/Flox}$; *Stra8-Cre* mice (referred to as *Stra8-*$Rnf20^{-/-}$) (Supplementary Figure S3D). Because the *Stra8*

promoter specifically expresses in early-stage spermatogonia from 3 days after birth onward, and peaks in preleptotene spermatocytes first present at postnatal day 7 (35), *Rnf20* exons 2–4 were specifically deleted in the germ cells, which was predicted to disrupt the open reading frame of *Rnf20* mRNA, thus resulting in germ cell-specific *Rnf20*-knockout mice. We first used immunoblotting to test *Rnf20*-knockout efficiency in *Stra8-Rnf20*$^{-/-}$ mice. As shown in Figure 1A, the protein level of RNF20 was dramatically reduced in the testes of the *Stra8-Rnf20*$^{-/-}$ mice compared with those of the *Rnf20*$^{Flox/Flox}$ and *Stra8-Rnf20*$^{+/-}$mice, suggesting that *Rnf20* was efficiently removed in the testes of the *Stra8-Rnf20*$^{-/-}$ mice. Most strikingly, the testes of the *Stra8-Rnf20*$^{-/-}$ mice were smaller than those of the *Rnf20*$^{Flox/Flox}$ and *Stra8-Rnf20*$^{+/-}$ mice (Figure 1B), and the testis weight of the *Stra8-Rnf20*$^{-/-}$ mice was reduced compared with that of the *Rnf20*$^{Flox/Flox}$ and *Stra8-Rnf20*$^{+/-}$mice (Figure 1C). Histological examination showed that the seminiferous tubule diameter of the *Stra8-Rnf20*$^{-/-}$ mouse was less than half of the *Rnf20*$^{Flox/Flox}$ mouse seminiferous tubule (Figure 1D and E). The *Stra8-Rnf20*$^{-/-}$ male mice lost most of their germ cells and possessed no round or elongated spermatids in the seminiferous tubules, and almost no mature spermatozoa were found in the epididymal lumens of these mice (Figure 1E and F). The breeding assays showed that the *Stra8-Rnf20*$^{-/-}$ male mice were completely infertile (Supplementary Figure S4). These results demonstrate that germ cell-specific *Rnf20* knockout results in spermatogenesis failure and suggest that *Rnf20* is essential for spermatogenesis.

Rnf20 knockout results in pachytene stage arrest in male mice

To determine exactly which stage of spermatogenesis was affected by *Rnf20* knockout, we used immunohistochemistry of the germ cell marker VASA to characterize the first wave of spermatogenesis in mice at 9 dpp (days postpartum), when testes begin to generate leptotene spermatocytes, at 12 dpp, when testes are populated by leptotene and zygotene spermatocytes, and at 15 dpp, when testes begin to generate pachytene spermatocytes. Compared with those of littermate controls, the seminiferous tubules of *Stra8-Rnf20*$^{-/-}$ mice contained similar numbers of germ cells at 9 dpp, but these numbers started to decrease at 12 dpp and dramatically dropped at 15 dpp (Figure 2A–C), suggesting that the *Rnf20* knockout affected the prophase of meiosis I. To define the exact block stage of *Stra8-Rnf20*$^{-/-}$ testis during spermatogenesis, PAS and hematoxylin staining were used to further analyse the phenotype of *Stra8-Rnf20*$^{-/-}$ testes. We found that the spermatogenesis was blocked at stage IV, and most of the spermatocytes arrested at the pachytene stage in the *Stra8-Rnf20*$^{-/-}$ testes (Supplementary Figure S5A). Some spermatocytes survived in the stage IV but then died in stage XII (Supplementary Figure S5A). The TUNEL assays results showed that these germ cells underwent apoptosis in the *Stra8-Rnf20*$^{-/-}$ seminiferous tubules (Supplementary Figure S5B-D). We further detected the exact meiotic stages which were affected by *Rnf20* knockout in spermatocyte nucleus spreads with an antibody against SYCP3, which is one of the SC components (10). In the control group, every prophase stage

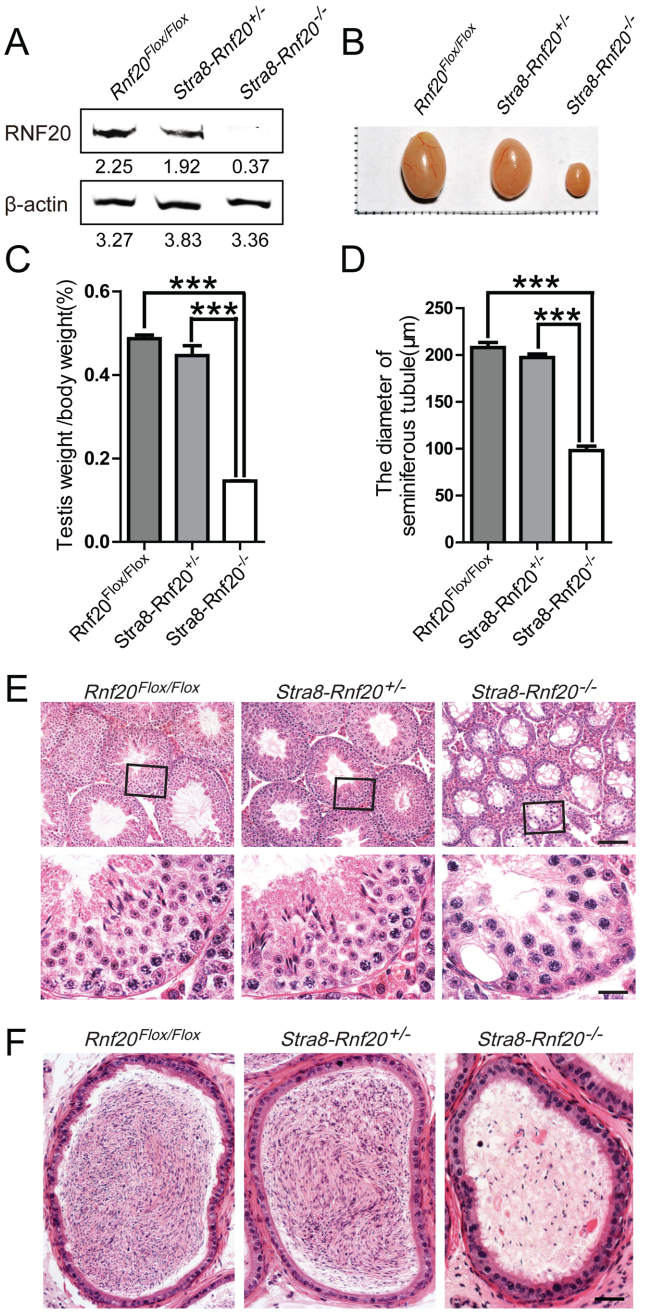

Figure 1. Spermatogenesis is disrupted in *Stra8-Rnf20*$^{-/-}$ mice. (**A**) The RNF20 protein level was dramatically reduced in the testes of the *Stra8-Rnf20*$^{-/-}$ mice. The numbers of the underlying bands were gray scale of RNF20 and β-actin quantified by the ODYSSEY Sa Infrared Imaging System. (**B**) The testes of the *Stra8-Rnf20*$^{-/-}$ mice were smaller than those of the *Rnf20*$^{Flox/Flox}$ mice. (**C**) The weight of the testes of the *Stra8-Rnf20*$^{-/-}$ mice was reduced compared with that of the *Rnf20*$^{Flox/Flox}$ mice. Testis weight/body weight: *Rnf20*$^{Flox/Flox}$, 0.49 ± 0.01; *Stra8-Rnf20*$^{+/-}$, 0.45 ± 0.02; *Stra8-Rnf20*$^{-/-}$, 0.15 ± 0.00. (**D**) The diameter of the seminiferous tubules in *Stra8-Rnf20*$^{-/-}$ mice was smaller than that in the *Stra8-Rnf2*$^{+/-}$ and *Rnf20*$^{Flox/Flox}$ mice. *Rnf20*$^{Flox/Flox}$, 202.1 ± 0.72 μm; *Stra8-Rnf2*$^{+/-}$, 198.6 ± 2.71 μm; *Stra8-Rnf20*$^{-/-}$, 96.63 ± 0.97 μm. (**E**) Histological analysis of the seminiferous tubules of the *Rnf20*$^{Flox/Flox}$, *Stra8-Rnf2*$^{+/-}$and *Stra8-Rnf20*$^{-/-}$mice. Scale bars, 100 μm, upper panel; 20 μm, lower panel. (**F**) Histological analysis of the caudal epididymides of the *Rnf20*$^{Flox/Flox}$, *Stra8-Rnf2*$^{+/-}$ and *Stra8-Rnf20*$^{-/-}$ mice. Scale bars, 50 μm. The *Rnf20*$^{Flox/Flox}$ and *Stra8-Rnf20*$^{-/-}$ mice in Figure 1 were 8 weeks old.

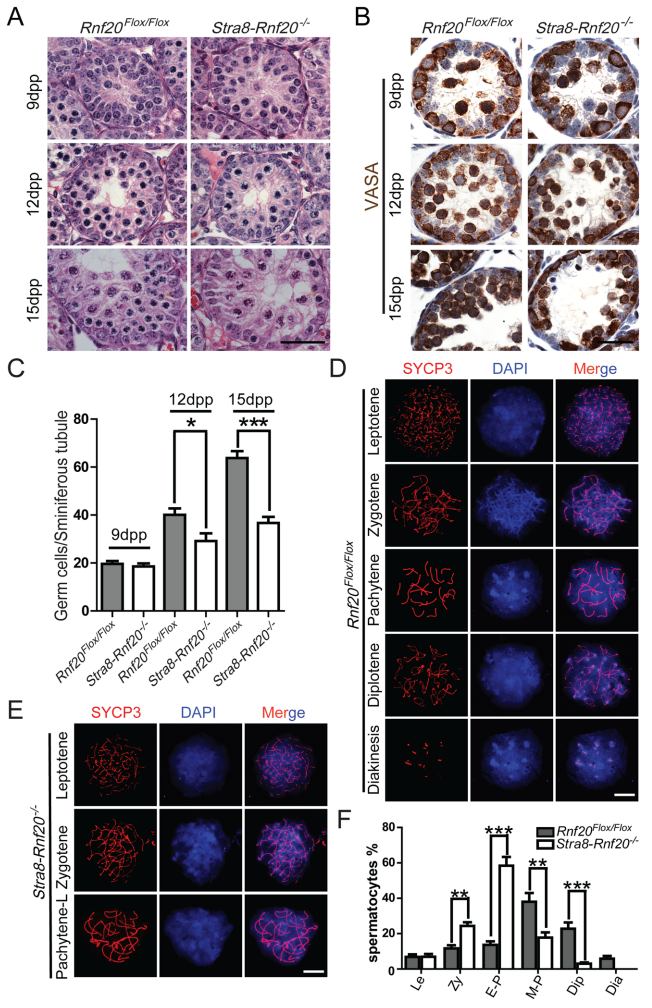

Figure 2. Meiosis arrests at the pachytene stage in *Stra8-Rnf20*$^{-/-}$ mouse testis. (**A**) Histological analysis of the seminiferous tubules of juvenile *Rnf20*$^{Flox/Flox}$ and *Stra8-Rnf20*$^{-/-}$ mice (9–15 dpp). Scale bars, 50 μm. (**B**) VASA immunohistochemical analysis of the germ cells in juvenile *Rnf20*$^{Flox/Flox}$ and *Stra8-Rnf20*$^{-/-}$ mice showed that the amount of the germ cells began to drop from 12 dpp to 15 dpp. Scale bars, 50 μm. (**C**) Quantification of the germ cells in the seminiferous tubules of the juvenile *Rnf20*$^{Flox/Flox}$ and *Stra8-Rnf20*$^{-/-}$mice in (B). 9 dpp: *Rnf20*$^{Flox/Flox}$, 19.63 ± 1.19; *Stra8-Rnf20*$^{-/-}$, 18.56 ± 1.27. 12 dpp: *Rnf20*$^{Flox/Flox}$, 40.08 ± 2.69; *Stra8-Rnf20*$^{-/-}$, 29.15 ± 3.19. 15 dpp: *Rnf20*$^{Flox/Flox}$, 63.77 ± 2.85; *Stra8-Rnf20*$^{-/-}$, 36.69 ± 2.52. (**D**, **E**) Meiotic chromosome spreads from *Rnf20*$^{Flox/Flox}$ and *Stra8-Rnf20*$^{-/-}$ males were stained with antibody to SYCP3. Scale bars, 10 μm. (**F**) Frequencies of meiotic stages in *Rnf20*$^{Flox/Flox}$ and *Stra8-Rnf20*$^{-/-}$testis suspensions. Le (Leptotene): *Rnf20*$^{Flox/Flox}$, 6.80 ± 1.53%; *Stra8-Rnf20*$^{-/-}$, 6.90 ± 1.62%. Zy (Zygotene): *Rnf20*$^{Flox/Flox}$, 11.60 ± 1.86%; *Stra8-Rnf20*$^{-/-}$, 24.40 ± 2.02%. E-P (Early-Pachytene): *Rnf20*$^{Flox/Flox}$, 13.60 ± 2.02%; *Stra8-Rnf20*$^{-/-}$, 58.40 ± 4.94%. M-P (Middle-Pachytene): *Rnf20*$^{Flox/Flox}$, 38.00 ± 4.97%; *Stra8-Rnf20*$^{-/-}$, 17.80 ± 2.91%. Dip (Diplotene): *Rnf20*$^{Flox/Flox}$, 22.80 ± 3.51%; *Stra8-Rnf20*$^{-/-}$, 3.60 ± 1.21%. Dia (Diakinesis): *Rnf20*$^{Flox/Flox}$, 5.80 ± 1.56%; *Stra8-Rnf20*$^{-/-}$, 0.00 ± 0.00%. The *Rnf20*$^{Flox/Flox}$ and *Stra8-Rnf20*$^{-/-}$ mice in Figure 2D-F were 8 weeks old.

could be identified (Figure 2D), whereas in the testes of the *Stra8-Rnf20*$^{-/-}$ mice, only those spermatocytes from the leptotene to pachytene stages were observed (Figure 2E). The proportion of the zygotene and early pachytene spermatocytes increased substantially, and some impaired mid-pachytene spermatocytes were observed in the *Stra8-Rnf20*$^{-/-}$ seminiferous tubules (Figure 2F). All these results suggest that *Rnf20* knockout leads to spermatocyte arrest at the pachytene stage, and this phenotype is irrelevant to its age.

Meiotic recombination is impaired in *Stra8-Rnf20*$^{-/-}$ spermatocytes

Defects in meiotic recombination are important causes for pachytene arrest (45). Meiotic recombination is dependent on the successful repair of programmed DSBs. MLH1, SYCP1, RPA1, RAD51and DMC1 are important marker molecules for different stages of meiotic recombination. RPA1 associates with single-strand intermediates and RAD51/DMC1 facilitate the invasion of homologous chromosomes (46). SYCP1 is one of the key components of the synaptonemal complex, and it bridges homologous chromosomes for recombination (10). MLH1 represents crossovers during meiotic recombination (11). When we monitored these markers via spermatocyte nuclear spreads and immunofluorescence, we found that MLH1 foci decreased dramatically due to the depletion of *Rnf20* in pachytene spermatocytes (Figure 3A and B), suggesting failed crossover formation. SYCP1 signals were not continuous in the *Rnf20*-depleted spermatocytes at the pachytene stage, suggesting that synapses were not fully assembled (Figure 3C, D and Supplementary Figure S6). RAD51 and DMC1 were not sufficiently recruited to the recombination foci in *Stra8-Rnf20*$^{-/-}$ spermatocytes (Figure 3E–H and Supplementary Figure S7A and B), suggesting a defect in programmed DSB repair. In *Stra8-Rnf20*$^{-/-}$ spermatocytes, both RPA1 and BRCA1 signals at the zygotene stage were decreased in comparison with those in *Rnf20*$^{Flox/Flox}$ spermatocytes (Figure 3G, H and Supplementary Figure S7C–G), suggesting defects in single strand DNA invasion or generation. All of these results suggest that the pachytene stage arrest that was caused by *Rnf20* depletion is associated with defects in meiotic homologous recombination and synapsis which are coupled with programmed DSB repair.

Effect of *Rnf20* knockout on programmed DSB repair in spermatocytes

To further investigate the functional role of RNF20 in programmed DSB repair, we monitored the following repair steps by immunofluorescence: γH2AX is a meiotic marker that accumulates in the nucleus during the leptotene (distributed globally) and zygotene stages (begin to disappear), concomitantly with DSB formation and repair, but decreases in the autosomes after DSB repair at the pachytene stage (concentrated in the XY body) (Figure 4A and Supplementary Figure S8A and B, upper three panels) (47). The X and Y chromosomes retain γH2AX at the pachytene stage most likely because these chromosomes lack homology and cannot fully undergo synapsis (Figure 4A and Supplementary Figure S8A and B) (47). At the leptotene stage, the γH2AX signals in *Stra8-Rnf20*$^{-/-}$ spermatocytes were modestly weaker than in *Rnf20*$^{Flox/Flox}$ spermatocytes (Supplementary Figure S8C). However, during the pachytene stage, the γH2AX signals in *Stra8-Rnf20*$^{-/-}$ spermatocytes were still diffused in the autosomes, rather

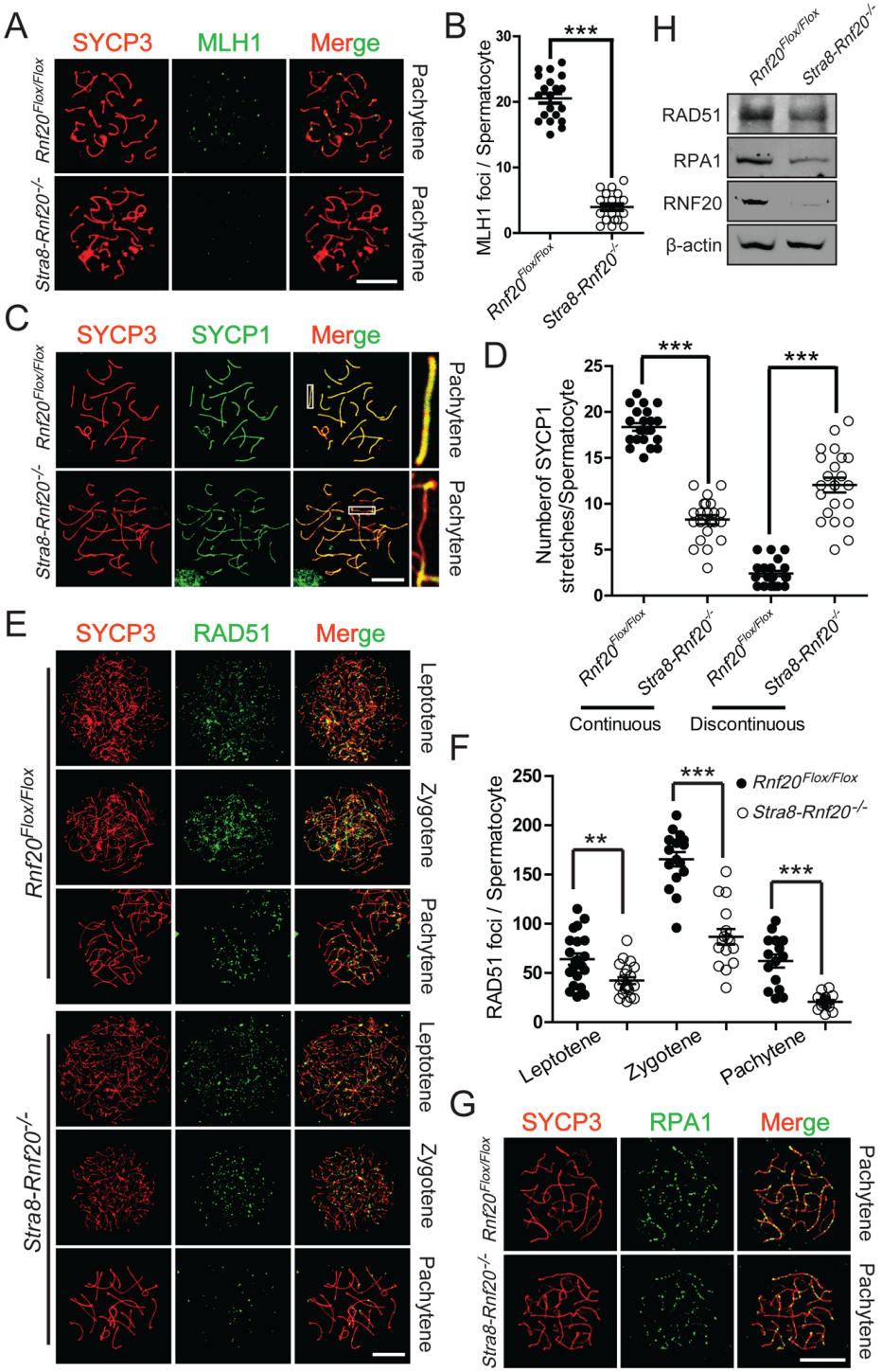

Figure 3. Meiotic crossover, synapsis, and strand invasion are impaired due to RNF20 depletion. (**A**) *Rnf20*$^{Flox/Flox}$ and *Stra8-Rnf20*$^{-/-}$ spermatocytes stained for SYCP3 (red) and MLH1 (green). Scale bars, 10 μm. (**B**) Quantification of the MLH1 foci number per cell in *Rnf20*$^{Flox/Flox}$ and *Stra8-Rnf20*$^{-/-}$ mice. *Rnf20*$^{Flox/Flox}$, 20.55 ± 0.75; *Stra8-Rnf20*$^{-/-}$, 3.95 ± 0.48. (**C**) *Rnf20*$^{Flox/Flox}$ and *Stra8-Rnf20*$^{-/-}$ spermatocytes stained for SYCP3 (red) and SYCP1 (green). Discontinuous SYCP1 staining was observed in *Stra8-Rnf20*$^{-/-}$ cells. Scale bars, 10 μm. (**D**) Number of SYCP1 stretches per *Rnf20*$^{Flox/Flox}$ or *Stra8-Rnf20*$^{-/-}$spermatocyte. Continuous SYCP1 stretches: *Rnf20*$^{Flox/Flox}$, 18.36 ± 0.41; *Stra8-Rnf20*$^{-/-}$, 8.27 ± 0.48. Discontinuous SYCP1 stretches: *Rnf20*$^{Flox/Flox}$, 2.41 ± 0.28; *Stra8-Rnf20*$^{-/-}$, 12.05 ± 0.81. (**E**) Spermatocytes stained for SYCP3 (red) and RAD51 (green) from *Rnf20*$^{Flox/Flox}$ and *Stra8-Rnf20*$^{-/-}$ mice. (**F**) Quantification of the RAD51 foci per cell in *Rnf20*$^{Flox/Flox}$ and *Stra8-Rnf20*$^{-/-}$ mice. Leptotene stage: *Rnf20*$^{Flox/Flox}$, 64.14 ± 5.70; *Stra8-Rnf20*$^{-/-}$, 42.33 ± 3.50. Zygotene stage: *Rnf20*$^{Flox/Flox}$, 165.40 ± 7.28; *Stra8-Rnf20*$^{-/-}$, 86.75 ± 7.92. Pachytene stage: *Rnf20*$^{Flox/Flox}$, 62.13 ± 6.67; *Stra8-Rnf20*$^{-/-}$, 20.81 ± 1.84. (**G**) Spermatocytes stained for SYCP3 (red) and RPA1 (green) in *Rnf20*$^{Flox/Flox}$ and *Stra8-Rnf20*$^{-/-}$ mice. RPA1 was not sufficiently recruited to the chromosomes in the *Stra8-Rnf20*$^{-/-}$ spermatocytes. Scale bars, 10 μm. (H) Immunoblot results showed decreased RAD51 and RPA1 in *Stra8-Rnf20*$^{-/-}$ spermatocytes. The *Rnf20*$^{Flox/Flox}$ and *Stra8-Rnf20*$^{-/-}$ spermatocytes used for immunofluorescence and western blottings were from 8 weeks mice.

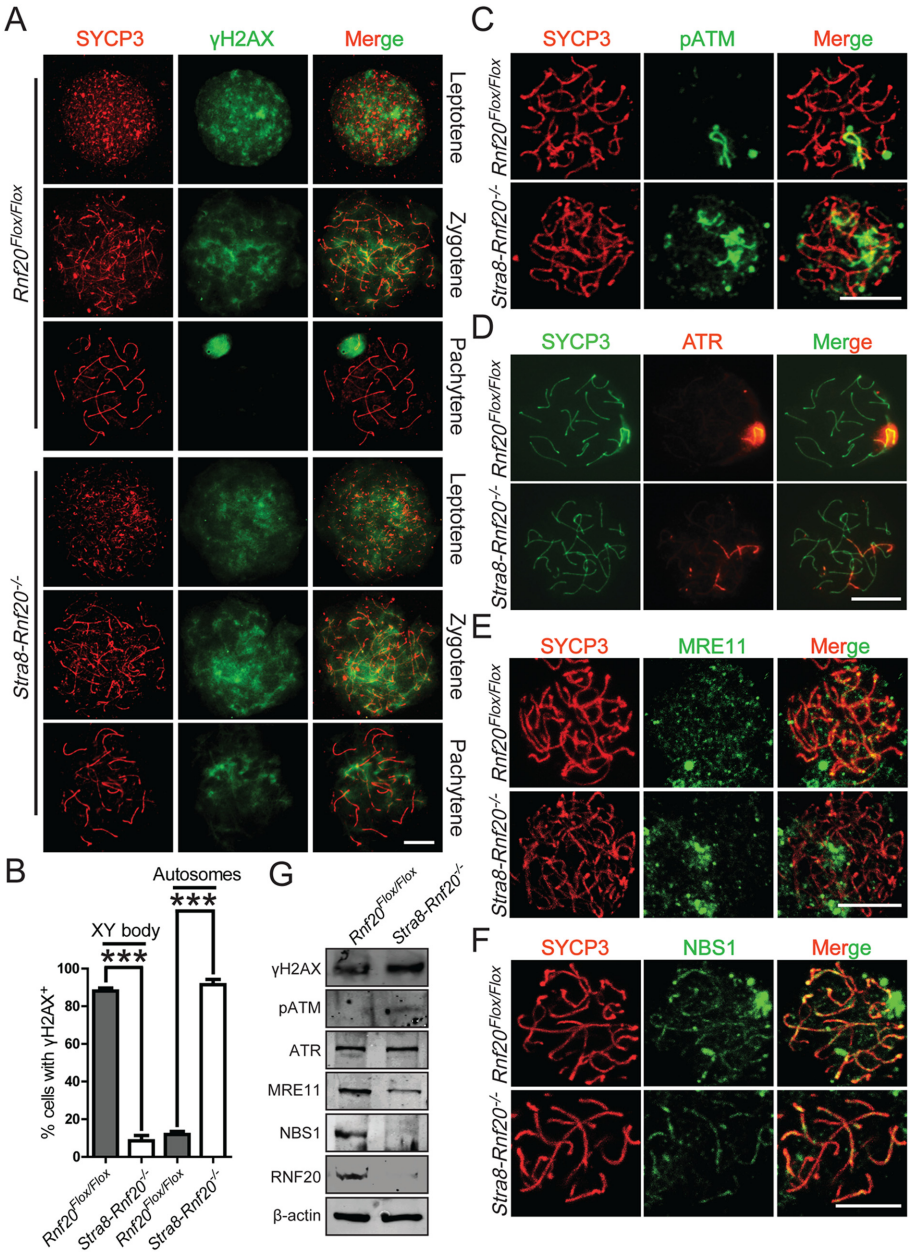

Figure 4. Programmed DSBs are not repaired efficiently due to the insufficient recruitment of repair factors in *Stra8-Rnf20*$^{-/-}$ spermatocytes. (**A**) *Rnf20*$^{Flox/Flox}$ and *Stra8-Rnf20*$^{-/-}$ spermatocytes stained for SYCP3 (red) and γH2AX (green). At the pachytene stage, γH2AX remained at some autosomal locations in *Stra8-Rnf20*$^{-/-}$ cells. (**B**) Percentage of cells retaining γH2AX outside of the sex chromosomes in *Rnf20*$^{Flox/Flox}$ and *Stra8-Rnf20*$^{-/-}$ pachytene spermatocytes. γH2AX signal localized on the XY bodies only: *Rnf20*$^{Flox/Flox}$, 88.11 ± 1.62%; *Stra8-Rnf20*$^{-/-}$, 8.510 ± 2.83%. γH2AX signal localized on the autosomes: *Rnf20*$^{Flox/Flox}$, 11.89 ± 1.62%; *Stra8-Rnf20*$^{-/-}$, 91.49 ± 2.83%. (**C**) Spermatocytes stained for SYCP3 (red) and pATM (green). In *Stra8-Rnf20*$^{-/-}$, the pATM signal was retained on the autosomes. Scale bars, 10 μm. (**D**) Spermatocytes stained for SYCP3 (green) and ATR (red). The ATR signal was retained on the autosomes in *Stra8-Rnf20*$^{-/-}$mice. (**E**) Spermatocytes stained for SYCP3 (red) and MRE11 (green) in *Rnf20*$^{Flox/Flox}$ and *Stra8-Rnf20*$^{-/-}$ mice. MRE11 was not sufficiently recruited onto the chromosomes in *Stra8-Rnf20*$^{-/-}$ spermatocytes. (**F**) Spermatocytes stained for SYCP3 (red) and NBS1 (green) in *Rnf20*$^{Flox/Flox}$ and *Stra8-Rnf20*$^{-/-}$ mice. NBS1 was not sufficiently recruited onto the chromosomes in *Stra8-Rnf20*$^{-/-}$ spermatocytes. (**G**) Immunoblot analysis of γH2AX, pATM, ATR, MRE11 and NBS1 in *Rnf20*$^{Flox/Flox}$ and *Stra8-Rnf20*$^{-/-}$ spermatocytes. Scale bars, 10 μm. The *Rnf20*$^{Flox/Flox}$ and *Stra8-Rnf20*$^{-/-}$ spermatocytes used for immunofluorescence and western blottings were from 8 weeks mice.

than accumulating only on the XY body (Figure 4A, B, G and Supplementary Figure S8C). These results suggest that RNF20 might be involved in programmed DSB formation as reported in yeast (14). Consistent with γH2AX, pATM and ATR were present on the autosomes in *Stra8-Rnf20*$^{-/-}$ pachytene spermatocytes, but completely disappeared on the autosomes in *Rnf20*$^{Flox/Flox}$ pachytene spermatocytes (Figure 4C, D, G and Supplementary Figure S9). These results indicate that the programmed DSB repair process is indeed delayed in *Rnf20*-knockout spermatocytes. Next, we compared the MRE11/RAD50/NBS1 (MRN) complex, which is involved in DSB end resectioning, of *Stra8-Rnf20*$^{-/-}$ spermatocytes with that of *Rnf20*$^{Flox/Flox}$ spermatocytes. As shown in Figure 4E–G and Supplementary Figure S10, MRE11 and NBS1 decreased dramatically in *Stra8-Rnf20*$^{-/-}$ spermatocytes, suggesting that the MRN complex might be insufficiently recruited to the programmed DSB sites in *Stra8-Rnf20*$^{-/-}$ spermatocytes. All of these results suggest that RNF20 might participate in MRN complex recruitment during programmed DSB end resectioning.

RNF20-mediated H2B ubiquitination promotes chromatin relaxation during meiosis

It has been reported that NBS1 directly interacts with RNF20 (21). Because NBS1 localizes on the chromosome at the prophase of meiosis I, RNF20, together with its partner RNF40, might also be recruited to the chromosome at this stage. To test this possibility, we used immunofluorescence to determine the subcellular localization of both proteins at the zygotene and pachytene stages; both RNF20 and RNF40 localized in the nucleus and were distributed in a thread-like structure (Supplementary Figure S11A and B). Both proteins co-localized well with SYCP3 (Figure 5A and B), suggesting they were indeed recruited to the chromosome at this stage. When the RNF20-positive thread-like structures disappeared in *Stra8-Rnf20*$^{-/-}$ spermatocytes (Supplementary Figure S11A), the RNF40 signal was also reduced (Supplementary Figure S11B). These results were further confirmed by immunoblotting (Figure 5C and Supplementary Figure S11C). At the same time, we found that the major product of RNF20/RNF40 H2Bub was also dramatically reduced (Figure 5C and Supplementary Figure S11D). All of these results suggest that RNF20 regulates meiotic recombination by mediating H2B ubiquitination.

RNF20-mediated H2B ubiquitination might regulate meiotic recombination by affecting chromatin structure. To test this possibility, we first determined the acetylation status of H3K14 (H3K14ac), which is an active transcription histone marker and is highly associated with programmed DSB hot spots during meiosis (Supplementary Figure S12A) (48,49). Interestingly, the total level of H3K14ac was reduced dramatically in *Stra8-Rnf20*$^{-/-}$ spermatocytes (Figure 5D-F). Because H3K14ac is directly involved in regulating chromatin relaxation (49–51), we then used a micrococcal nuclease (MNase) sensitivity assay to determine how RNF20-mediated H2B ubiquitination regulates chromatin structure during meiotic recombination. We found that *Stra8-Rnf20*$^{-/-}$ chromosomes were more resistant to MNase digestion than *Rnf20*$^{Flox/Flox}$ chromosomes during the zygotene and pachytene stages (Figure 5G and H), suggesting that H2B ubiquitination promotes chromatin relaxation during these stages. In support of the above conclusions, we found that a heterochromatin-associated modification, dimethylation at histone H3K9 (H3K9me2) (Supplementary Figure S12B) (51–53), was increased significantly at these stages (Figure 5D, I and J), further confirming the changes in chromatin structure. All of these results suggest that RNF20-mediated H2B ubiquitination relaxes the chromatin structure at the programmed DSB sites during meiosis, allowing the recruitment of DSB repair factors to the proper position.

The spermatogenetic defect of *Stra8-Rnf20*$^{-/-}$ mice can be partially rescued by forced chromatin relaxation

If RNF20-mediated H2B ubiquitination regulates meiotic recombination by promoting chromatin relaxation, then forced chromatin relaxation might at least partially rescue meiotic recombination or even the spermatogenetic defect of *Stra8-Rnf20*$^{-/-}$ mice. To test this possibility, we injected 30 μl of 93.8–156.3 μM chloroquine, which can alter chromatin and chromosome structures (54), into 6-week-old mouse testes and studied the effects 3 weeks later. Injection of 156.3 μM chloroquine clearly destroyed the spermatogenesis process in *Rnf20*$^{Flox/Flox}$ mice, while the lower dose of 93.8 μM chloroquine did not result in any observable effect on *Rnf20*$^{Flox/Flox}$ mouse testes (Figure 6A and Supplementary Figure S13A). However, the injection of 93.8 μM chloroquine into the testes of *Stra8-Rnf20*$^{-/-}$ mice restored spermatogenesis to some extent; round, elongated spermatids and some mature spermatozoa were observed in some *Stra8-Rnf20*$^{-/-}$ mouse seminiferous tubules (Figure 6A), and the number of germ cells and the diameter of the seminiferous tubules also increased significantly (Figure 6B and C). Immunostaining results confirmed that the expression and localization of NBS1 and RAD51 were restored to some extent in spermatocytes of *Stra8-Rnf20*$^{-/-}$ mice after chloroquine injection (Figure 6D and E), suggesting that meiotic recombination was partially rescued. Furthermore, western blotting results of H3K14ac (marker of loosed chromatin) and H3K4me2 (marker of condensed chromatin) showed that the chloroquine treatment indeed partially restored the chromatin relaxation status of RNF20 deficient spermatocytes (Supplementary Figure S13B-D). Finally, histological examination of the epididymal lumens and total spermatozoa analysis showed that chloroquine injection into the testes of *Stra8-Rnf20*$^{-/-}$ mice significantly increased the numbers of mature spermatozoa in the epididymis (Figure 6F and G and Supplementary Figure S13E). These results demonstrate that chloroquine can partially rescue the spermatogenetic defect of *Stra8-Rnf20*$^{-/-}$ mice by relaxing the chromatin structure and thus restoring impaired meiotic recombination.

H2B ubiquitination mediated chromatin relaxation is required for meiosis

Next, we tested whether a deficiency of H2B ubiquitination is really responsible for the meiotic defect in *Rnf20* knockout cells. Because of a technical obstacle to create

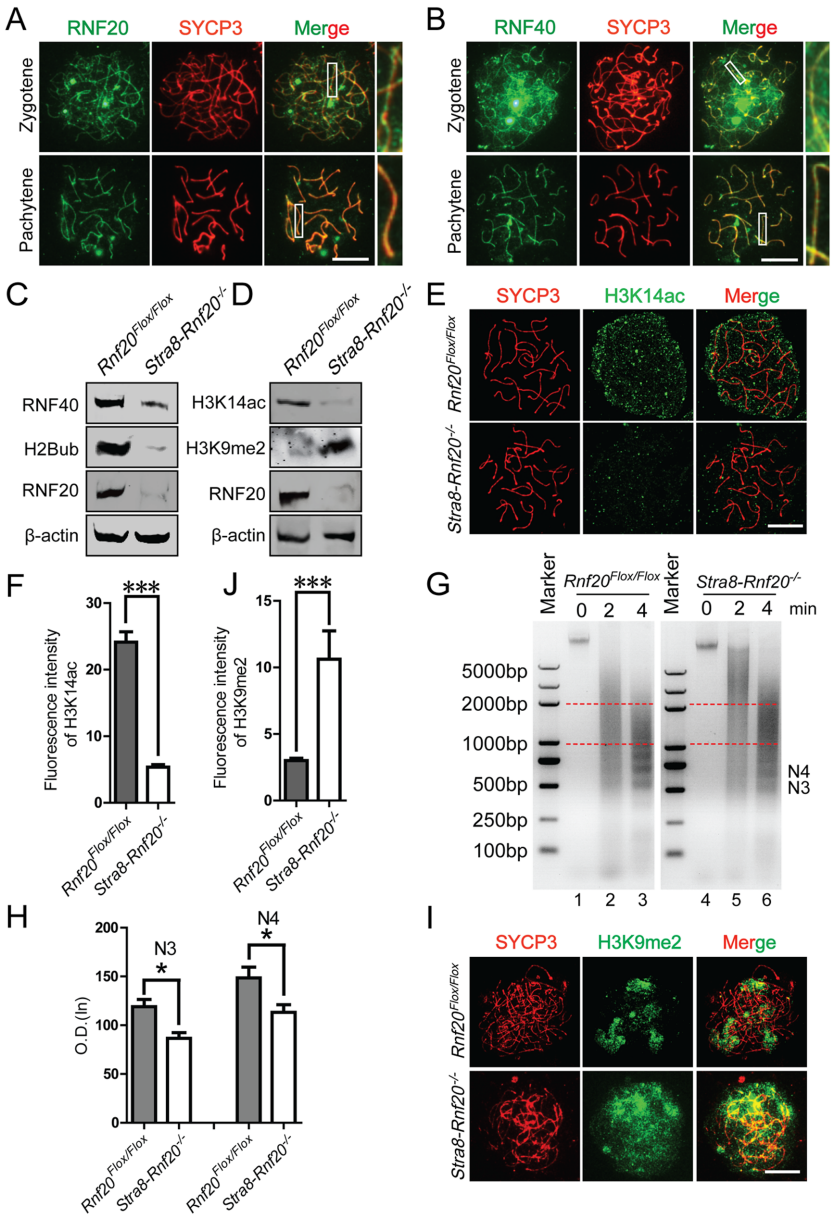

Figure 5. RNF20 modulates meiotic recombination by promoting chromatin relaxation. (**A** and **B**) Spermatocytes stained for SYCP3 (red) and RNF20/RNF40 (green) in wild-type mice. RNF20 and RNF40 were recruited onto the chromosomes at the zygotene and pachytene stages. (**C**) Immunoblot analysis of RNF40 and H2Bub in *Rnf20*$^{Flox/Flox}$ and *Stra8-Rnf20*$^{-/-}$ spermatocytes. RNF40 and H2Bub were decreased significantly in *Stra8-Rnf20*$^{-/-}$ spermatocytes. (**D**) Immunoblot analysis of H3K14ac and H3K9me2 in *Rnf20*$^{Flox/Flox}$ and *Stra8-Rnf20*$^{-/-}$ spermatocytes. (**E**) Spermatocytes stained for SYCP3 (red) and H3K14ac (green) in *Rnf20*$^{Flox/Flox}$ and *Stra8-Rnf20*$^{-/-}$ mice. H3K14ac was decreased in *Stra8-Rnf20*$^{-/-}$ spermatocytes. (**F**) Relative fluorescence intensity of H3K14ac in *Rnf20*$^{Flox/Flox}$ and *Stra8-Rnf20*$^{-/-}$spermatocytes. *Rnf20*$^{Flox/Flox}$, 24.14 ± 1.55; *Stra8-Rnf20*$^{-/-}$, 5.35 ± 0.39. (**G**) Chromatin isolated from *Stra8-Rnf20*$^{-/-}$ spermatocytes was more compacted than chromatin isolated from *Rnf20*$^{Flox/Flox}$ spermatocytes. Micrococcal nuclease (MNase) sensitivity assay was used to detect the chromatin compaction status which was isolated from *Rnf20*$^{Flox/Flox}$ and *Stra8-Rnf20*$^{-/-}$ spermatocytes. (**H**) Quantification of the N3 and N4 intensities of lanes 3 and 6 in (G) using GIS 1D software; N3 and N4 indicate the number of nucleosomes. N3: *Rnf20*$^{Flox/Flox}$, 119.00 ± 7.44; *Stra8-Rnf20*$^{-/-}$, 86.50 ± 5.85. N4: *Rnf20*$^{Flox/Flox}$, 148.50 ± 11.00; *Stra8-Rnf20*$^{-/-}$, 113.3 ± 7.86. (**I**) Spermatocytes stained for SYCP3 (red) and H3K9me2 (green) in *Rnf20*$^{Flox/Flox}$ and *Stra8-Rnf20*$^{-/-}$ mice. H3K9me2 was increased in *Stra8-Rnf20*$^{-/-}$ spermatocytes. (J) Relative fluorescence intensity of H3K9me2 in *Rnf20*$^{Flox/Flox}$ and *Stra8-Rnf20*$^{-/-}$ spermatocytes: *Rnf20*$^{Flox/Flox}$, 3.01 ± 0.17; *Stra8-Rnf20*$^{-/-}$, 10.62 ± 2.12. Scale bars, 10 μm.The *Rnf20*$^{Flox/Flox}$ and *Stra8-Rnf20*$^{-/-}$ spermatocytes used for immunofluorescence, western blottings and MNase assay were from 8 weeks mice.

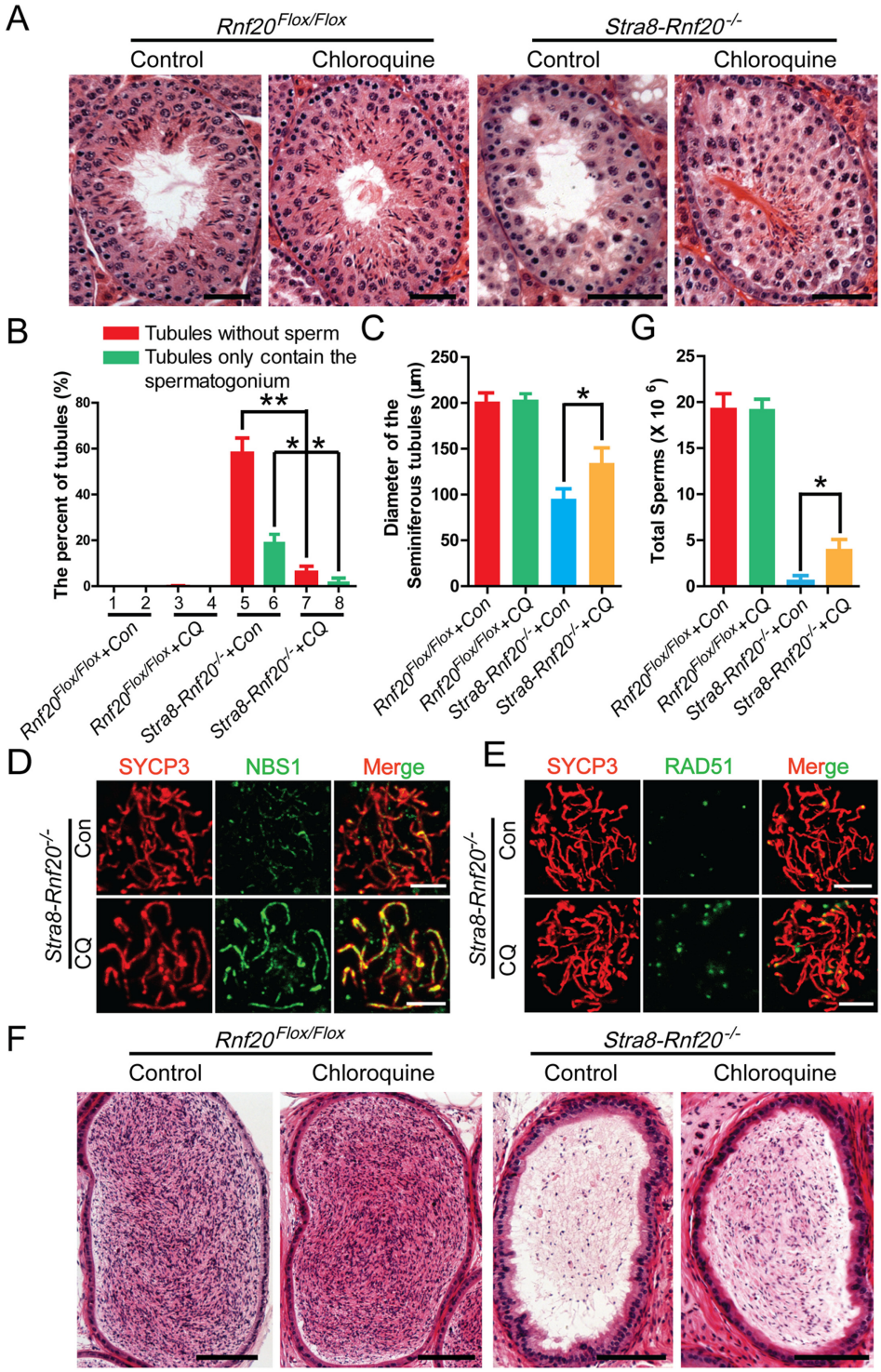

Figure 6. Chloroquine partially rescues meiotic recombination and spermatogenetic processes in *Stra8-Rnf20*$^{-/-}$ mice. (**A**) Histological analysis of the seminiferous tubules of the *Rnf20*$^{Flox/Flox}$ and *Stra8-Rnf20*$^{-/-}$ mice after injection with or without CQ (93.8 μM chloroquine) into each testis. Scale bars, 50 μm. (**B**) Quantification of the seminiferous tubules in (A). The seminiferous tubules containing only spermatogonia: *Stra8-Rnf20*$^{-/-}$ + Con, 58.27 ± 6.33%; *Stra8-Rnf20*$^{-/-}$ + CQ, 6.37 ± 2.32%. The seminiferous tubules without spermatozoa: *Stra8-Rnf20*$^{-/-}$ + Con, 19.39 ± 2.29%; *Stra8-Rnf20*$^{-/-}$ + CQ, 1.99 ± 0.81%. (**C**) Diameters of the seminiferous tubules in (A): *Rnf20*$^{Flox/Flox}$+ Con, 201.6 ± 6.63 μm; *Rnf20*$^{Flox/Flox}$+ CQ, 203.1 ± 5.42 μm; *Stra8-Rnf20*$^{-/-}$ + Con, 93.13 ± 9.19 μm; *Stra8-Rnf20*$^{-/-}$ + CQ, 139.4 ± 15.07 μm. (**D**, **E**) Spermatocytes stained for SYCP3 (red) and NBS1 or RAD51 (green) after injection with or without CQ (93.8 μM chloroquine). (**F**) Histological analysis of the epididymides of the *Rnf20*$^{Flox/Flox}$ and *Stra8-Rnf20*$^{-/-}$ mice after injection with or without CQ (93.8 μM chloroquine). Scale bars, 100 μm. (**G**) The total number of spermatozoa from the caudal epididymides of the *Rnf20*$^{Flox/Flox}$ and *Stra8-Rnf20*$^{-/-}$ mice after injection with or without CQ (93.8 μM chloroquine). *Rnf20*$^{Flox/Flox}$ + Con, 19.34 ± 1.40 × 10^6; *Rnf20*$^{Flox/Flox}$ + CQ, 19.27 ± 0.87 × 10^6; *Stra8-Rnf20*$^{-/-}$ + Con, 0.60 ± 0.21 × 10^6; *Stra8-Rnf20*$^{-/-}$ + CQ, 4.03 ± 0.87 × 10^6. The chloroquine treatmented mice were 6 weeks.

H2B K120R mutant mouse, we turned to yeast to test this possibility. H2B K123 was ubiquitinated by the homologue of RNF20/RNF40, Bre1p, to modulate gene transcription and meiotic DSB formation in yeast (14,55). To that end, we created a *Bre1* deletion mutant yeast strain, we found that the sporulation efficiency decreased dramatically compared with a wild-type control strain (Figure 7A and Supplementary Figure S14A). Interestingly, the addition of chloroquine to the media during the first 4 h not only relaxed the chromatin (Figure 7B and C), but also restored the sporulation efficiency to some extent (Figure 7A and Supplementary Figure S14A). Consistent with these results, the *H2BK123R* strain almost completely failed to sporulate (Figure 7D and Supplementary Figure S14B), while the addition of chloroquine to the media significantly increased both the chromatin sensitivity to MNase (Figure 7E and F) and the sporulation efficiency of this mutant strain (Figure 7D and Supplementary Figure S14B). These results suggest that, in addition to programmed DSB production (14), Bre1p mediated H2B ubiquitination also regulates meiotic recombination by promoting chromatin relaxation in yeast, and may share the similar functional role to RNF20/RNF40-mediated H2B ubiquitination during mammalian meiotic recombination. These findings indicate that the RNF20/Bre1p mediated H2B ubiquitination could maintain an accessible meiotic chromatin structure to guarantee the timely repair of programmed DSBs and the finishing of the meiotic recombination.

DISCUSSION

H2B ubiquitination regulates numerous molecular and cellular processes, such as transcription elongation (27), DNA replication (56), DNA damage response (21,24), nucleosome dynamics (57), chromatin segregation (58), centromeric chromatin maintenance (59), chromatin boundary integrity (60) and the activity of other histone-modifying enzymes (61,62). Although it has been reported that H2B ubiquitination is involved in stem cell differentiation (29,30), apoptosis (63) and tumorigenesis (26), its *in vivo* physiological and developmental functions have not been well investigated, especially in mammals, due to the absence of an animal model. To study the potential function of H2B ubiquitination during meiosis, we generated the first germ cell-specific *Rnf20*-knockout mouse and found that RNF20-mediated H2B ubiquitination regulates meiotic recombination by promoting chromatin relaxation and facilitating the recruitment of some early DNA repair factors to the chromatin. Previously, it has been reported that H2B ubiquitination is required for the recruitment of a DSB-creating complex at specific loci during meiosis, rather than having a general effect on DSB formation in budding yeast (14). Although we found that RNF20-mediated H2B ubiquitination might also be involved in programmed DSB formation in mammals, its major function still is to regulate meiotic recombination since almost all RNF20 deficient spermatocytes arrest at pachytene stage. In contrast to the above, mutations in the plant orthologs of mammalian *Rnf20*/*Rnf40*, *Hub1* and *Hub2* only caused a reduction in seed dormancy and plant size in *Arabidopsis* (64,65), suggesting H2B ubiquitination may not be essential for meiotic recombination at all. Thus, although the essential components of H2B ubiquitination are evolutionarily conserved, the functional role of H2B ubiquitination in mammalian meiotic recombination is distinct from those in plants, suggesting that meiotic recombination is different from somatic cell homologous recombination at this point, and the latter is evolutionary conserved from yeast to vertebrates (21).

During the DNA damage response in somatic cells, RNF20 interacts with both ATM and NBS1 at the DSB sites, but *Rnf20* knockdown does not affect the NBS1 signal at the DSB sites during homologous recombinational repair (21,24). However, during meiotic recombination, RPA1, DMC1, MRE11, and NBS1, but not pATM and ATR, decreased dramatically in *Stra8-Rnf20*$^{-/-}$ spermatocytes (Figures 3G, H, 4C–G and Supplementary Figure S7, S9, S10), a result that was entirely different from that of homologous recombination in somatic cells. The decreasing presence of these proteins is likely due to failed recruitment to the programmed DSB sites, thus making them unstable, but not due to a transcriptional defect because we did not observe a clear decrease in their mRNA levels (Supplementary Figure S15). It has been reported that H2B ubiquitination leads to an open and biochemically accessible fiber conformation (66). Accordingly, the major function of H2B ubiquitination during meiotic recombination is to relax chromosome structures and facilitate the recruitment of some meiotic recombination factors to the programmed DSB sites. This conclusion is supported by our observation that chromatins from *Stra8-Rnf20*$^{-/-}$ spermatocytes, *bre1Δ* and *H2BK123R* yeast strains are resistant to MNase digestion, and that forced chromatin relaxation partially rescues the gametogenesis defect of *Rnf20*-deficient spermatocytes, *bre1Δ* and *H2BK123R* yeast cells (Figures 5G, H and 7C-F). Interestingly, forced chromatin relaxation partially restored the recruitment of not only RAD51 but also NBS1 to the chromatin of *Stra8-Rnf20*$^{-/-}$ spermatocytes (Figure 6D and E); this result suggests that, in addition to RNF20, at least one other unknown protein can recruit NBS1 to the chromatin under these conditions. Although we cannot exclude the possibility that the MRN complex on the chromatin becomes unstable in the absence of *Rnf20* during meiotic recombination, we favor the scenario that once programmed DSB has occurred, ATM recruits RNF20 to ubiquitinate H2B. Simultaneously or subsequently, RNF20 or another unknown protein recruits the MRN complex to the programmed DSB sites on the decondensed chromatin, followed by other DNA repair factors to finish the entire meiotic recombination process (Figure 8A).

In this study, once *Rnf20* was knocked out, the chromatin could not be relaxed. Consequently, the MRN complex and other DNA repair factors could not be efficiently recruited to the programmed DSB sites, and those DSBs could not be repaired by meiotic recombination, resulting in spermatocyte cell death and ultimately male infertility in mice (Figure 8B). In addition to H2B ubiquitination, it has been reported that the posttranslational modification status of H3 and H4 are involved in meiosis by de-condensing local chromatin structures to regulate meiotic recombination (67,68). Actually, in addition to histone modifications, some components of the chromatin remod-

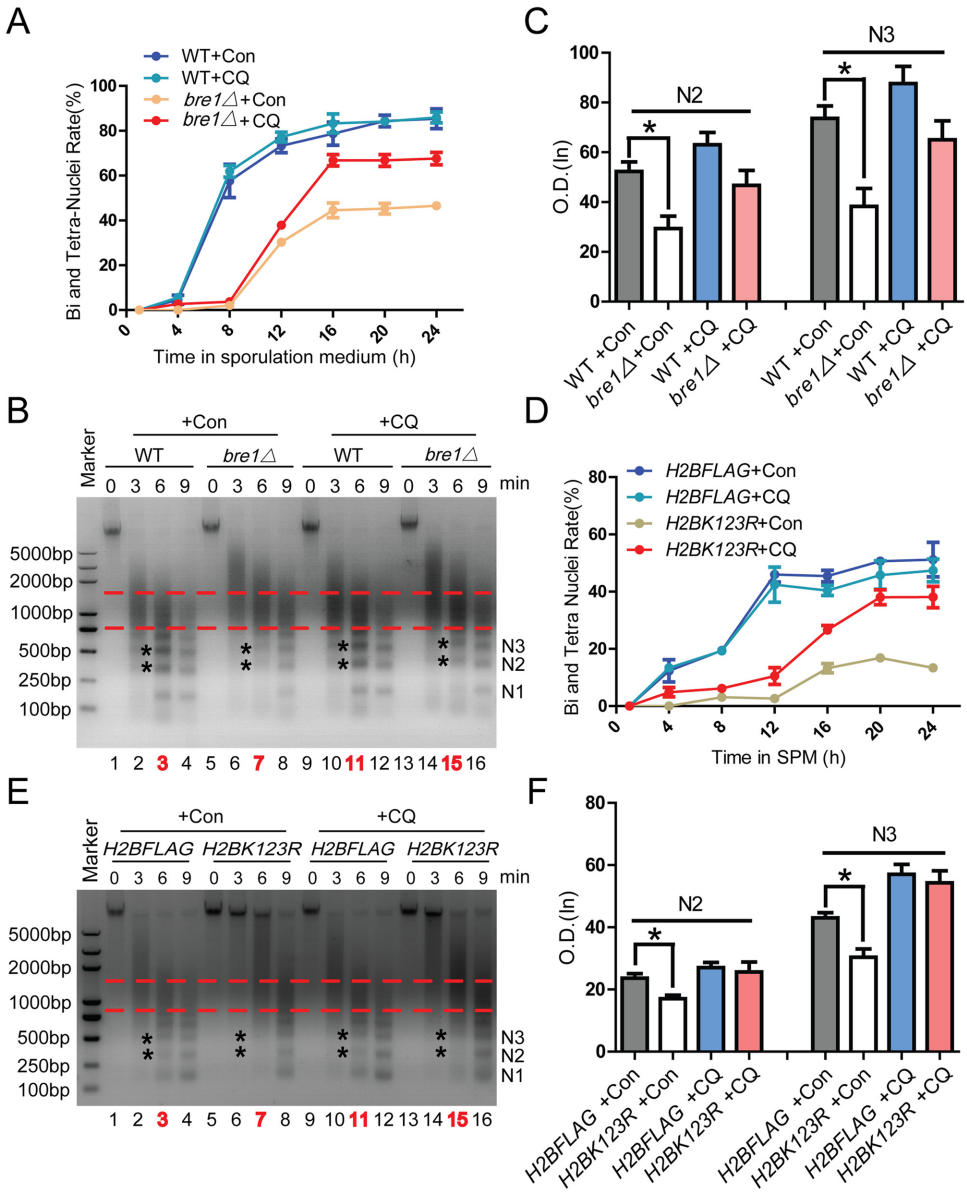

Figure 7. H2B ubiquitination regulates chromatin condensation status during yeast meiosis. (**A**) Chloroquine (CQ) treatment partially rescued the sporulation defect of the *bre1Δ* (Bre1 deficient) yeast strain. *bre1Δ* yeast strain was induced to sporulate at the presence or absence of 93.8 μM CQ condition. The cells were collected at the indicated time points, and stained with 4′,6-diamidino-2- phenylindole (DAPI), the percentage of cells/asci with dyads and tetrads were counted on the fluorescent microscopy. (**B**) Effect of *bre1* deletion and CQ treatment on chromatin condensation status at the pachytene stage of meiosis I (The fourth hour of the sporulation). Micrococcal Nuclease (MNase) Assay was used to detect the chromatin condensation status of the cells in (A) at fourth hour (pachytene stage). After fixation and extraction, the chromatins from the above mentioned cells were digested with MNase, the mononucleotides and oligonucleotides were detected by agarose gel electrophoresis and ethidium bromide staining. (**C**) Quantification of N2 and N3 intensities of lanes 3, 7, 11 and 15 in (B) by using GIS 1D software. N2 and N3 indicate the number of nucleosomes. N2: WT + Con, 52.33 ± 3.76; *bre1Δ* + Con, 29.33 ± 5.04; WT + CQ, 63.00 ± 4.93; *bre1Δ* + CQ, 46.67 ± 6.01. N3: WT + Con, 73.67 ± 4.98; *bre1Δ* + Con, 38.33 ± 7.13; WT + CQ, 87.67 ± 6.89; *bre1Δ* + CQ, 65.00 ± 7.64. (**D**) Chloroquine (CQ) treatment partially rescued the sporulation defect of the *H2BK123R* (H2B ubiquitination deficient yeast strain) yeast strain. The CQ treatment and sporulation assays were similar to (A). (**E**) Effect of H2B ubiquitination and CQ treatment on chromatin condensation status at the pachytene stage of meiosis I. Micrococcal Nuclease (MNase) Assay was used to detect the chromatin condensation status of the cells in (D). (**F**) Quantification of N2 and N3 intensities of lanes 3, 7, 11 and 15 in (E) by using GIS 1D software. N2 and N3 indicate the number of nucleosomes. N2: *H2BFLAG* + Con, 23.67 ± 1.45; *H2BK123R* + Con, 17.00 ± 1.16; *H2BFLAG* + CQ, 27.00 ± 1.73; *H2BK123R* + CQ, 25.67 ± 3.18. N3: *H2BFLAG* + Con, 43.00 ± 1.73; *H2BK123R* + Con, 30.33 ± 2.67; *H2BFLAG* + CQ, 57.00 ± 3.22; *H2BK123R* + CQ, 54.33 ± 3.84.

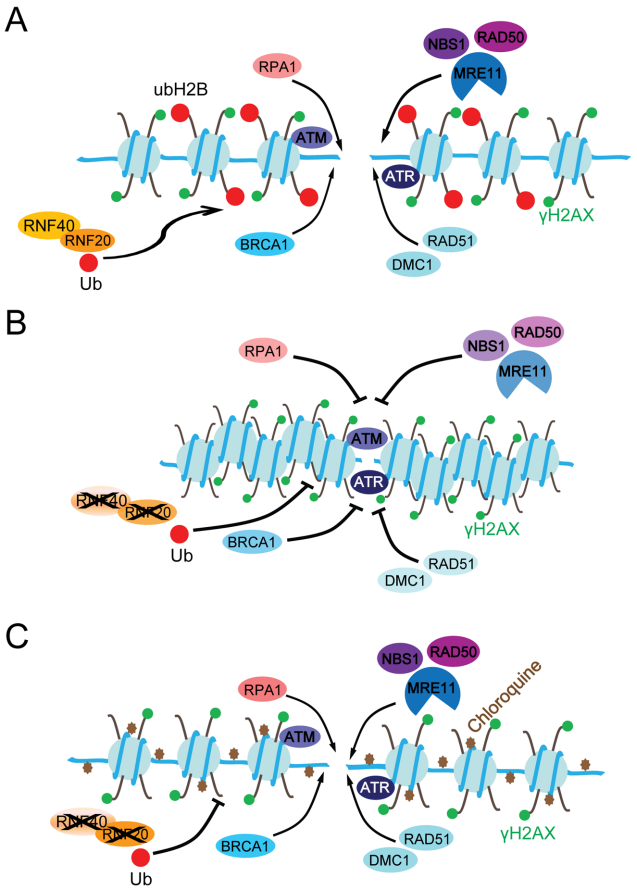

Figure 8. Diagrams of the proposed functional roles of RNF20-mediated H2B ubiquitination and chloroquine during meiotic recombination. (**A**) In the initiation of programmed DSB repair, ATM and ATR recruit RNF20 to ubiquitinate H2B and promote chromatin relaxation. Simultaneously or subsequently, RNF20 or another unknown protein recruits the MRN (MRE11/RAD50/NBS1) complex to the programmed DSB sites on the de-condensed chromatin, followed by other DNA repair factors such as RPA1, BRCA1 RAD51 and DMC1 to finish the entire meiotic recombination process. (**B**) In the RNF20-deficient spermatocytes, H2B cannot be ubiquitinated. As such, meiotic chromatin cannot be relaxed, which affects the efficient recruitment of the MRN complex (MRE11/RAD50/NBS1) and other DNA repair factors (RPA1, BRCA1, RAD51 and DMC1) to the DSB sites. Thereafter, programmed DSBs cannot be repaired by meiotic recombination, resulting in spermatocyte cell death and ultimately male infertility in mice. (**C**) During meiotic recombination in *Stra8-Rnf20*$^{-/-}$ spermatocytes, the insertion of chloroquine into the chromatin may relax the chromatin, mimicking the function of H2B ubiquitination. Thus, the recruitment of repair and recombination factors is partially restored, which recovers the programmed DSB repair and meiotic homologous recombination in the *Rnf20*-deficient spermatocytes and partially rescues spermatogenesis in *Stra8-Rnf20*$^{-/-}$ mice.

eling complexes, such as switching defective/sucrose nonfermenting (SWI/SNF), imitation switch (ISWI), chromodomain, helicase, and DNA binding (CHD) and inositol requiring 80 (INO80), might also be involved in chromatin relaxation during meiotic recombination; an ATPase subunit of SWI/SNF, brahma-related gene 1 (*Brg1*), has been found to be required for meiotic recombination in mice (51). Thus, we speculate that in addition to the action of these well-studied factors, the involvement of many chromatin relaxation-related factors in meiotic recombination might be uncovered in the near future.

Meiotic recombination is essential for fertility and the integrity of the genome (69). Reduced or absent meiotic recombination may lead to spermatogenic arrest, which results in male infertility (69,70). The *Rnf20*-knockout mouse model produces a phenotype that is very similar to some cases of human oligozoospermia or azoospermia. Although there are no reported *Rnf20*- or *Rnf40*-associated male infertility patients, the existence of these types of patients should not be discounted. Even if *Rnf20*-associated patients do not exist, the existence of chromatin relaxation defect-associated male infertility is very likely. Most importantly, we found that the meiotic recombination and spermatogenesis defects of *Stra8-Rnf20*$^{-/-}$ mice were partially rescued by the injection of a 4-aminoquinoline drug that has long been used in the treatment or prevention of malaria (71). Chloroquine is also a chromatin relaxation agent that can intercalate into the nuclear strands and force chromatin relaxation (54). During meiotic recombination in *Stra8-Rnf20*$^{-/-}$ spermatocytes or *H2BK123R* yeast cells, the insertion of chloroquine into meiotic chromatin might relax the chromatin, which can mimic the function of H2B ubiquitination, thus partially restoring the meiotic recombination process (Figure 8C). Together with the fact that low-dosage chloroquine can partially rescue some homologous recombination defects in somatic cells (21,22), we predict that this drug might be applied to the treatment of some chromatin relaxation defect-associated reproductive or even other kinds of diseases, and this old drug may greet its bright spring again in the future.

SUPPLEMENTARY DATA

Supplementary Data are available at NAR Online.

ACKNOWLEDGEMENTS

We thank Jun Huang, Liangran Zhang, Kehkooi Kee and Linyu Lu for their critical reading of the manuscript. We are grateful to Shangying Liao for testis injection.
Author contributions: Z.X. performed most of the experiments; Z.S., G.L., H.T., W.L., Y.L., P.W., Y.W., X.C., C.L. and Y.S. performed some of the experiments; Z.X., D.G.d.R., F.G. and W.L. analyzed the data; W.L. initiated the project and designed the experiments; W.L. and Z.X. wrote the paper. All authors read and approved the final manuscript.

FUNDING

National key R&D program of China [2016YFA0500901]; National Natural Science Foundation of China [91519317, 31171374]. Funding for open access charge: National Natural Science Foundation of China [91519317, 31171374].
Conflict of interest statement. None declared.

REFERENCES

1. Nagaoka,S.I., Hassold,T.J. and Hunt,P.A. (2012) Human aneuploidy: mechanisms and new insights into an age-old problem. *Nat. Rev. Genet.*, **13**, 493–504.

2. Page,S.L. and Hawley,R.S. (2003) Chromosome choreography: the meiotic ballet. *Science*, **301**, 785–789.
3. Keeney,S., Giroux,C.N. and Kleckner,N. (1997) Meiosis-specific DNA double-strand breaks are catalyzed by Spo11, a member of a widely conserved protein family. *Cell*, **88**, 375–384.
4. Ciccia,A. and Elledge,S.J. (2010) The DNA damage response: making it safe to play with knives. *Mol. Cell*, **40**, 179–204.
5. Ward,I.M. and Chen,J. (2001) Histone H2AX is phosphorylated in an ATR-dependent manner in response to replicational stress. *J. Biol. Chem.*, **276**, 47759–47762.
6. Cousineau,I., Abaji,C. and Belmaaza,A. (2005) BRCA1 regulates RAD51 function in response to DNA damage and suppresses spontaneous sister chromatid replication slippage: implications for sister chromatid cohesion, genome stability, and carcinogenesis. *Cancer Res.*, **65**, 11384–11391.
7. Wu,X., Ranganathan,V., Weisman,D.S., Heine,W.F., Ciccone,D.N., O'Neill,T.B., Crick,K.E., Pierce,K.A., Lane,W.S., Rathbun,G. *et al.* (2000) ATM phosphorylation of Nijmegen breakage syndrome protein is required in a DNA damage response. *Nature*, **405**, 477–482.
8. Borde,V. (2007) The multiple roles of the Mre11 complex for meiotic recombination. *Chromosome Res.*, **15**, 551–563.
9. Tarsounas,M., Morita,T., Pearlman,R.E. and Moens,P.B. (1999) RAD51 and DMC1 form mixed complexes associated with mouse meiotic chromosome cores and synaptonemal complexes. *J. Cell Biol.*, **147**, 207–220.
10. Zickler,D. and Kleckner,N. (1999) Meiotic chromosomes: integrating structure and function. *Annu. Rev. Genet.*, **33**, 603–754.
11. Guillon,H., Baudat,F., Grey,C., Liskay,R.M. and de Massy,B. (2005) Crossover and noncrossover pathways in mouse meiosis. *Mol. Cell*, **20**, 563–573.
12. Kohl,K.P. and Sekelsky,J. (2013) Meiotic and mitotic recombination in meiosis. *Genetics*, **194**, 327–334.
13. Bekker-Jensen,S. and Mailand,N. (2011) The ubiquitin- and SUMO-dependent signaling response to DNA double-strand breaks. *FEBS Lett.*, **585**, 2914–2919.
14. Yamashita,K., Shinohara,M. and Shinohara,A. (2004) Rad6-Bre1-mediated histone H2B ubiquitylation modulates the formation of double-strand breaks during meiosis. *Proc. Natl. Acad. Sci. U.S.A.*, **101**, 11380–11385.
15. Kwon,Y.T., Xia,Z., An,J.Y., Tasaki,T., Davydov,I.V., Seo,J.W., Sheng,J., Xie,Y. and Varshavsky,A. (2003) Female lethality and apoptosis of spermatocytes in mice lacking the UBR2 ubiquitin ligase of the N-end rule pathway. *Mol. Cell. Biol.*, **23**, 8255–8271.
16. Kopanja,D., Roy,N., Stoyanova,T., Hess,R.A., Bagchi,S. and Raychaudhuri,P. (2011) Cul4A is essential for spermatogenesis and male fertility. *Dev. Biol.*, **352**, 278–287.
17. Qiao,H., Prasada Rao,H.B., Yang,Y., Fong,J.H., Cloutier,J.M., Deacon,D.C., Nagel,K.E., Swartz,R.K., Strong,E., Holloway,J.K. *et al.* (2014) Antagonistic roles of ubiquitin ligase HEI10 and SUMO ligase RNF212 regulate meiotic recombination. *Nat. Genet.*, **46**, 194–199.
18. Zhao,G.Y., Sonoda,E., Barber,L.J., Oka,H., Murakawa,Y., Yamada,K., Ikura,T., Wang,X., Kobayashi,M., Yamamoto,K. *et al.* (2007) A critical role for the ubiquitin-conjugating enzyme Ubc13 in initiating homologous recombination. *Mol. Cell*, **25**, 663–675.
19. Ma,T., Keller,J.A. and Yu,X. (2011) RNF8-dependent histone ubiquitination during DNA damage response and spermatogenesis. *Acta Biochim. Biophys. Sinica*, **43**, 339–345.
20. Bohgaki,M., Bohgaki,T., El Ghamrasni,S., Srikumar,T., Maire,G., Panier,S., Fradet-Turcotte,A., Stewart,G.S., Raught,B., Hakem,A. *et al.* (2013) RNF168 ubiquitylates 53BP1 and controls its response to DNA double-strand breaks. *Proc. Natl. Acad. Sci. U.S.A.*, **110**, 20982–20987.
21. Nakamura,K., Kato,A., Kobayashi,J., Yanagihara,H., Sakamoto,S., Oliveira,D.V., Shimada,M., Tauchi,H., Suzuki,H., Tashiro,S. *et al.* (2011) Regulation of homologous recombination by RNF20-dependent H2B ubiquitination. *Mol. Cell*, **41**, 515–528.
22. Oliveira,D.V., Kato,A., Nakamura,K., Ikura,T., Okada,M., Kobayashi,J., Yanagihara,H., Saito,Y., Tauchi,H. and Komatsu,K. (2014) Histone chaperone FACT regulates homologous recombination by chromatin remodeling through interaction with RNF20. *J. Cell Sci.*, **127**, 763–772.
23. Zhang,F. and Yu,X. (2011) WAC, a functional partner of RNF20/40, regulates histone H2B ubiquitination and gene transcription. *Mol. Cell*, **41**, 384–397.
24. Moyal,L., Lerenthal,Y., Gana-Weisz,M., Mass,G., So,S., Wang,S.Y., Eppink,B., Chung,Y.M., Shalev,G., Shema,E. *et al.* (2011) Requirement of ATM-dependent monoubiquitylation of histone H2B for timely repair of DNA double-strand breaks. *Mol. Cell*, **41**, 529–542.
25. Zhu,B., Zheng,Y., Pham,A.D., Mandal,S.S., Erdjument-Bromage,H., Tempst,P. and Reinberg,D. (2005) Monoubiquitination of human histone H2B: the factors involved and their roles in HOX gene regulation. *Mol. Cell*, **20**, 601–611.
26. Shema,E., Tirosh,I., Aylon,Y., Huang,J., Ye,C., Moskovits,N., Raver-Shapira,N., Minsky,N., Pirngruber,J., Tarcic,G. *et al.* (2008) The histone H2B-specific ubiquitin ligase RNF20/hBRE1 acts as a putative tumor suppressor through selective regulation of gene expression. *Genes Dev.*, **22**, 2664–2676.
27. Pavri,R., Zhu,B., Li,G., Trojer,P., Mandal,S., Shilatifard,A. and Reinberg,D. (2006) Histone H2B monoubiquitination functions cooperatively with FACT to regulate elongation by RNA polymerase II. *Cell*, **125**, 703–717.
28. Wozniak,G.G. and Strahl,B.D. (2014) Catalysis-dependent stabilization of Bre1 fine-tunes histone H2B ubiquitylation to regulate gene transcription. *Genes Dev.*, **28**, 1647–1652.
29. Fuchs,G., Shema,E., Vesterman,R., Kotler,E., Wolchinsky,Z., Wilder,S., Golomb,L., Pribluda,A., Zhang,F., Haj-Yahya,M. *et al.* (2012) RNF20 and USP44 regulate stem cell differentiation by modulating H2B monoubiquitylation. *Mol. Cell*, **46**, 662–673.
30. Karpiuk,O., Najafova,Z., Kramer,F., Hennion,M., Galonska,C., Konig,A., Snaidero,N., Vogel,T., Shchebet,A., Begus-Nahrmann,Y. *et al.* (2012) The histone H2B monoubiquitination regulatory pathway is required for differentiation of multipotent stem cells. *Mol. Cell*, **46**, 705–713.
31. Buszczak,M., Paterno,S. and Spradling,A.C. (2009) Drosophila stem cells share a common requirement for the histone H2B ubiquitin protease scrawny. *Science*, **323**, 248–251.
32. Johnsen,S.A. (2012) The enigmatic role of H2Bub1 in cancer. *FEBS Lett.*, **586**, 1592–1601.
33. Liu,P., Jenkins,N.A. and Copeland,N.G. (2003) A highly efficient recombineering-based method for generating conditional knockout mutations. *Genome Res.*, **13**, 476–484.
34. Rodriguez,C.I., Buchholz,F., Galloway,J., Sequerra,R., Kasper,J., Ayala,R., Stewart,A.F. and Dymecki,S.M. (2000) High-efficiency deleter mice show that FLPe is an alternative to Cre-loxP. *Nat. Genet.*, **25**, 139–140.
35. Sadate-Ngatchou,P.I., Payne,C.J., Dearth,A.T. and Braun,R.E. (2008) Cre recombinase activity specific to postnatal, premeiotic male germ cells in transgenic mice. *Genesis*, **46**, 738–742.
36. Liu,Y.J., Liu,C., Chang,Z., Wadas,B., Brower,C.S., Song,Z.H., Xu,Z.L., Shang,Y.L., Liu,W.X., Wang,L.N. *et al.* (2016) Degradation of the separase-cleaved Rec8, a meiotic cohesin subunit, by the N-end rule pathway. *J. Biol. Chem.*, **291**, 7426–7438.
37. Peters,A.H., Plug,A.W., van Vugt,M.J. and de Boer,P. (1997) A drying-down technique for the spreading of mammalian meiocytes from the male and female germline. *Chromosome Res.*, **5**, 66–68.
38. Bellve,A.R., Cavicchia,J.C., Millette,C.F., O'Brien,D.A., Bhatnagar,Y.M. and Dym,M. (1977) Spermatogenic cells of the prepuberal mouse. Isolation and morphological characterization. *J. Cell Biol.*, **74**, 68–85.
39. Blank,M., Tang,Y., Yamashita,M., Burkett,S.S., Cheng,S.Y. and Zhang,Y.E. (2012) A tumor suppressor function of Smurf2 associated with controlling chromatin landscape and genome stability through RNF20. *Nat. Med.*, **18**, 227–234.
40. Hirota,K., Fukuda,T., Yamada,T. and Ohta,K. (2009) Analysis of chromatin structure at meiotic DSB sites in yeasts. *Methods Mol. Biol.*, **557**, 253–266.
41. Ogawa,T., Arechaga,J.M., Avarbock,M.R. and Brinster,R.L. (1997) Transplantation of testis germinal cells into mouse seminiferous tubules. *Int. J. Dev. Biol.*, **41**, 111–122.
42. Wach,A., Brachat,A., Pohlmann,R. and Philippsen,P. (1994) New heterologous modules for classical or PCR-based gene disruptions in Saccharomyces cerevisiae. *Yeast*, **10**, 1793–1808.
43. Robzyk,K., Recht,J. and Osley,M.A. (2000) Rad6-dependent ubiquitination of histone H2B in yeast. *Science*, **287**, 501–504.

44. Recht,J. and Osley,M.A. (1999) Mutations in both the structured domain and N-terminus of histone H2B bypass the requirement for Swi-Snf in yeast. *EMBO J.*, **18**, 229–240.
45. Barchi,M., Mahadevaiah,S., Di Giacomo,M., Baudat,F., de Rooij,D.G., Burgoyne,P.S., Jasin,M. and Keeney,S. (2005) Surveillance of different recombination defects in mouse spermatocytes yields distinct responses despite elimination at an identical developmental stage. *Mol. Cell. Biol.*, **25**, 7203–7215.
46. Baudat,F., Imai,Y. and de Massy,B. (2013) Meiotic recombination in mammals: localization and regulation. *Nat. Rev. Genet.*, **14**, 794–806.
47. Blanco-Rodriguez,J. (2012) Programmed phosphorylation of histone H2AX precedes a phase of DNA double-strand break-independent synapsis in mouse meiosis. *Reproduction*, **144**, 699–712.
48. Hansen,L., Kim,N.K., Marino-Ramirez,L. and Landsman,D. (2011) Analysis of biological features associated with meiotic recombination hot and cold spots in Saccharomyces cerevisiae. *PLoS One*, **6**, e29711.
49. Lee,H.S., Park,J.H., Kim,S.J., Kwon,S.J. and Kwon,J. (2010) A cooperative activation loop among SWI/SNF, gamma-H2AX and H3 acetylation for DNA double-strand break repair. *EMBO J.*, **29**, 1434–1445.
50. Wang,Y., Kallgren,S.P., Reddy,B.D., Kuntz,K., Lopez-Maury,L., Thompson,J., Watt,S., Ma,C., Hou,H., Shi,Y. *et al.* (2012) Histone H3 lysine 14 acetylation is required for activation of a DNA damage checkpoint in fission yeast. *J. Biol. Chem.*, **287**, 4386–4393.
51. Kim,Y., Fedoriw,A.M. and Magnuson,T. (2012) An essential role for a mammalian SWI/SNF chromatin-remodeling complex during male meiosis. *Development*, **139**, 1133–1140.
52. Rea,S., Eisenhaber,F., O'Carroll,D., Strahl,B.D., Sun,Z.W., Schmid,M., Opravil,S., Mechtler,K., Ponting,C.P., Allis,C.D. *et al.* (2000) Regulation of chromatin structure by site-specific histone H3 methyltransferases. *Nature*, **406**, 593–599.
53. Tachibana,M., Nozaki,M., Takeda,N. and Shinkai,Y. (2007) Functional dynamics of H3K9 methylation during meiotic prophase progression. *EMBO J.*, **26**, 3346–3359.
54. Mahut,M., Leitner,M., Ebner,A., Lammerhofer,M., Hinterdorfer,P. and Lindner,W. (2012) Time-resolved chloroquine-induced relaxation of supercoiled plasmid DNA. *Anal. Bioanal. Chem.*, **402**, 373–380.
55. Wood,A., Krogan,N.J., Dover,J., Schneider,J., Heidt,J., Boateng,M.A., Dean,K., Golshani,A., Zhang,Y., Greenblatt,J.F. *et al.* (2003) Bre1, an E3 ubiquitin ligase required for recruitment and substrate selection of Rad6 at a promoter. *Mol. Cell*, **11**, 267–274.
56. Trujillo,K.M. and Osley,M.A. (2012) A role for H2B ubiquitylation in DNA replication. *Mol. Cell*, **48**, 734–746.
57. Batta,K., Zhang,Z., Yen,K., Goffman,D.B. and Pugh,B.F. (2011) Genome-wide function of H2B ubiquitylation in promoter and genic regions. *Genes Dev.*, **25**, 2254–2265.
58. Latham,J.A., Chosed,R.J., Wang,S. and Dent,S.Y. (2011) Chromatin signaling to kinetochores: transregulation of Dam1 methylation by histone H2B ubiquitination. *Cell*, **146**, 709–719.
59. Sadeghi,L., Siggens,L., Svensson,J.P. and Ekwall,K. (2014) Centromeric histone H2B monoubiquitination promotes noncoding transcription and chromatin integrity. *Nat. Struct. Mol. Biol.*, **21**, 236–243.
60. Ma,M.K., Heath,C., Hair,A. and West,A.G. (2011) Histone crosstalk directed by H2B ubiquitination is required for chromatin boundary integrity. *PLoS Genet.*, **7**, e1002175.
61. Kim,J., Guermah,M., McGinty,R.K., Lee,J.S., Tang,Z., Milne,T.A., Shilatifard,A., Muir,T.W. and Roeder,R.G. (2009) RAD6-Mediated transcription-coupled H2B ubiquitylation directly stimulates H3K4 methylation in human cells. *Cell*, **137**, 459–471.
62. Wood,A., Schneider,J., Dover,J., Johnston,M. and Shilatifard,A. (2003) The Paf1 complex is essential for histone monoubiquitination by the Rad6-Bre1 complex, which signals for histone methylation by COMPASS and Dot1p. *J. Biol. Chem.*, **278**, 34739–34742.
63. Walter,D., Matter,A. and Fahrenkrog,B. (2010) Bre1p-mediated histone H2B ubiquitylation regulates apoptosis in Saccharomyces cerevisiae. *J. Cell Sci.*, **123**, 1931–1939.
64. Fleury,D., Himanen,K., Cnops,G., Nelissen,H., Boccardi,T.M., Maere,S., Beemster,G.T., Neyt,P., Anami,S., Robles,P. *et al.* (2007) The Arabidopsis thaliana homolog of yeast BRE1 has a function in cell cycle regulation during early leaf and root growth. *Plant Cell*, **19**, 417–432.
65. Liu,Y., Koornneef,M. and Soppe,W.J. (2007) The absence of histone H2B monoubiquitination in the Arabidopsis hub1 (rdo4) mutant reveals a role for chromatin remodeling in seed dormancy. *Plant Cell*, **19**, 433–444.
66. Fierz,B., Chatterjee,C., McGinty,R.K., Bar-Dagan,M., Raleigh,D.P. and Muir,T.W. (2011) Histone H2B ubiquitylation disrupts local and higher-order chromatin compaction. *Nat. Chem. Biol.*, **7**, 113–119.
67. Buard,J., Barthes,P., Grey,C. and de Massy,B. (2009) Distinct histone modifications define initiation and repair of meiotic recombination in the mouse. *EMBO J.*, **28**, 2616–2624.
68. Yamada,T. and Ohta,K. (2013) Initiation of meiotic recombination in chromatin structure. *J. Biochem.*, **154**, 107–114.
69. Hann,M.C., Lau,P.E. and Tempest,H.G. (2011) Meiotic recombination and male infertility: from basic science to clinical reality? *Asian J. Androl.*, **13**, 212–218.
70. Sun,F., Greene,C., Turek,P.J., Ko,E., Rademaker,A. and Martin,R.H. (2005) Immunofluorescent synaptonemal complex analysis in azoospermic men. *Cytogenet. Genome Res.*, **111**, 366–370.
71. Summers,R.L., Dave,A., Dolstra,T.J., Bellanca,S., Marchetti,R.V., Nash,M.N., Richards,S.N., Goh,V., Schenk,R.L., Stein,W.D. *et al.* (2014) Diverse mutational pathways converge on saturable chloroquine transport via the malaria parasite's chloroquine resistance transporter. *Proc. Natl. Acad. Sci. U.S.A.*, **111**, E1759–1767.